CELL BIOLOGY

# ATAT1-enriched vesicles promote microtubule acetylation via axonal transport

Aviel Even[1]*, Giovanni Morelli[2,3]*, Loïc Broix[2]*, Chiara Scaramuzzino[4,5], Silvia Turchetto[2], Ivan Gladwyn-Ng[2], Romain Le Bail[2], Michal Shilian[1], Stephen Freeman[2], Maria M. Magiera[6,7], A. S. Jijumon[6,7], Nathalie Krusy[2], Brigitte Malgrange[2], Bert Brone[3], Paula Dietrich[8], Ioannis Dragatsis[8], Carsten Janke[6,7], Frédéric Saudou[4,5,9], Miguel Weil[1]*†, Laurent Nguyen[2]*†



**Microtubules are polymerized dimers of α- and β-tubulin that underlie a broad range of cellular activities. Acetylation of α-tubulin by the acetyltransferase ATAT1 modulates microtubule dynamics and functions in neurons. However, it remains unclear how this enzyme acetylates microtubules over long distances in axons. Here, we show that loss of ATAT1 impairs axonal transport in neurons in vivo, and cell-free motility assays confirm a requirement of α-tubulin acetylation for proper bidirectional vesicular transport. Moreover, we demonstrate that the main cellular pool of ATAT1 is transported at the cytosolic side of neuronal vesicles that are moving along axons. Together, our data suggest that axonal transport of ATAT1-enriched vesicles is the predominant driver of α-tubulin acetylation in axons.**

## INTRODUCTION

Neurons are polarized cells, structurally and functionally divided into somatodendritic and axonal compartments. Axons are often long and characterized by intense bidirectional microtubule (MT)–dependent transport of cargos to control critical functions, including cell survival and neurotransmission. Cargos such as vesicles and membrane organelles (e.g., mitochondria, endosomes, and lysosomes) as well as proteins and messenger ribonucleoprotein complexes are loaded on molecular motors to undergo axonal transport along MTs. The anterograde transport is powered by the kinesin superfamily, while retrograde transport involves cytoplasmic dynein (*1*). Posttranslational modifications (PTMs) of MTs have been suggested to modulate axonal transport (*2*, *3*). Specifically, the acetylation of MTs may contribute to this process by enhancing the recruitment of kinesin and dynein and their mobility (*4*, *5*). Moreover, increasing MT acetylation improves the transport deficits resulting from mutations in *Huntingtin* and *LRRK2* genes (*4*, *6*). The acetylation of α-tubulin in MTs is driven by the α-tubulin *N*-acetyltransferase 1 (ATAT1)/MEC17 (*7*, *8*). Recent in vitro experiments performed with recombinant ATAT1 have suggested that it can enter the lumen of MTs from their extremities and/or lateral imperfection (*9*, *10*) and passively diffuses to promote acetylation of α-tubulin K40 residues (*11*, *12*). However, it remains unclear how ATAT1 reaches and acetylates MTs in living cells. This question is particularly important in neurons where axons and dendrites cover long distances with rather homogenously acetylated MTs. To decipher how ATAT1 promotes MT acetylation in neurons, we combined cell-free assays with cellular and molecular analyses of ex vivo (organotypic slices) or cultured mouse cortical projection neurons (in microfluidic chambers) and motoneurons of *Drosophila* larvae in vivo. Our work unveils the existence of a predominant pool of ATAT1 at the cytosolic side of motile vesicles, whose active transport promotes acetylation of α-tubulin in MTs. Therefore, we propose that the transport of ATAT1-enriched vesicles is a predominant driver of axonal MT acetylation.

## RESULTS

### Loss of Atat1 interferes with axonal transport in neurons across species

ATAT1 promotes the acetylation of α-tubulin in MTs, a PTM that favors the recruitment of kinesin and dynein and their mobility along axons (*4*, *5*, *13*). To test whether loss of Atat1 impairs axonal transport in cortical projection neurons in situ, we performed time-lapse recordings of organotypic brain slices from postnatal (P) day 2 wild-type (WT) mice. For this purpose, embryonic day 14.5 (E14.5) mouse embryos were in utero electroporated (IUE) with a combination of 4OH-tamoxifen (4OHT)–inducible Cre, Cre-inducible short hairpin RNA against Atat1 (shAtat1) (fig. S1A), Cre-inducible red fluorescent protein, and Lamp1-Emerald plasmids. Successive injections of 4OHT allowed us to identify the callosal projection of IUE neurons and record the transport of Lamp1-Emerald–positive lysosomes (Fig. 1, A and B, and movie S1). We showed that the 4OHT-induced knockdown (KD) of *Atat1* in callosal projection neurons 3 days after IUE at E14.5 (to maintain the expression of *Atat1* during the migration of projection neurons) impaired both anterograde and retrograde axonal transports recorded at P2 (Fig. 1, A to F, and fig. S1B). The KD of *Atat1* led to the reduction of the average and instantaneous velocities (Fig. 1, C and D) and the run length and to the increase of the pausing time of lysosomes (Fig. 1, E and F). These data were confirmed in cortical projection neurons from E14.5 *Atat1* knockout mice (*Atat1 KO*) or their corresponding WT controls (*14*) cultured for 5 days in vitro (DIV) in microfluidic devices and incubated with fluorescent probes to follow the transport of lysosomes and mitochondria along axonal MTs (Fig. 1, G and H, and movies S2 and S3). The average velocities

[1]Laboratory for Neurodegenerative Diseases and Personalized Medicine, Department of Cell Research and Immunology, The George S. Wise Faculty for Life Sciences, Sagol School of Neurosciences, Tel Aviv University, Ramat Aviv 69978, Israel. [2]GIGA-Stem Cells and GIGA-Neurosciences, Interdisciplinary Cluster for Applied Genoproteomics (GIGA-R), University of Liège, CHU Sart Tilman, Liège 4000, Belgium. [3]BIOMED Research Institute, University of Hasselt, Hasselt 3500, Belgium. [4]Grenoble Institut des Neurosciences, GIN, Univ. Grenoble Alpes, F-38000 Grenoble, France. [5]Inserm, U1216, F-38000 Grenoble, France. [6]Institut Curie, PSL Research University, CNRS UMR 3348, F-91405 Orsay, France. [7]Université Paris-Sud, Université Paris-Saclay, CNRS UMR3348, F-91405 Orsay, France. [8]Department of Physiology, University of Tennessee Health Science Center, Memphis, TN 38163, USA. [9]CHU Grenoble Alpes, F-38000 Grenoble, France.
*These authors contributed equally to this work.
†Corresponding author. Email: lnguyen@uliege.be (L.N.); miguelw@tauex.tau.ac.il (M.W.)

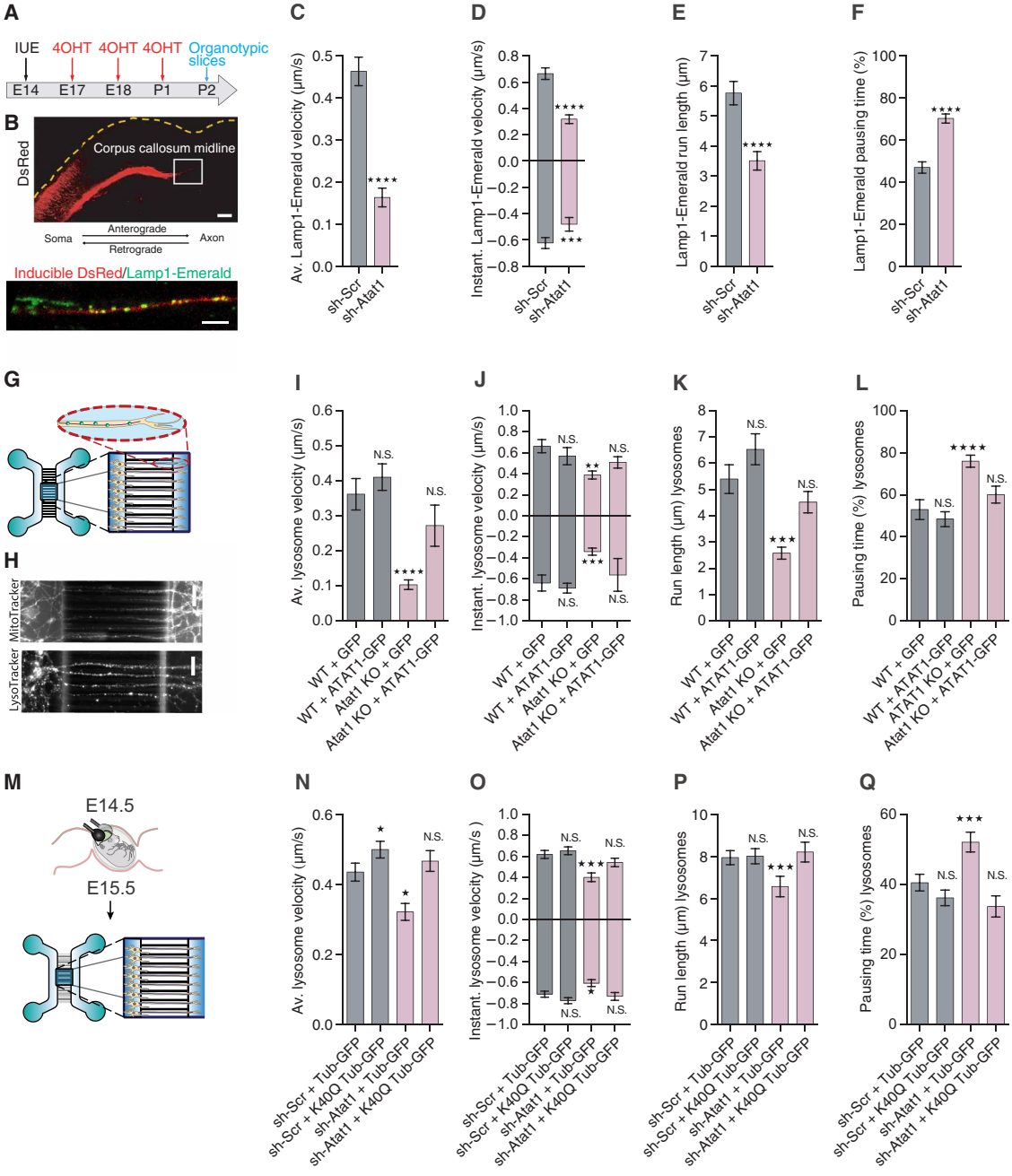


**Fig. 1. Depletion of Atat1 prevents acetylation of α-tubulin and interferes with fast axonal transport of organelles ex vivo and in vitro.** (**A**) Experimental setup used to perform axonal transport recordings in organotypic brain slice. (**B**) Labeling of lysosome Lamp1-Emerald$^{+}$ (green) and inducible dsRed (red) in axons crossing the corpus callosum of a P2 mouse cortical section. Scale bars, 200 μm (top) and 10 μm (bottom). (**C** to **F**) Histograms showing axonal transport parameters of Lamp1-Emerald (lysosomes) to analyze average velocity (C), instantaneous velocity (D), run length (E), and pausing time (F). (**G**) Microfluidic device setup used for recording axonal transport in cortical neurons. (**H**) Labeling of lysosomes and mitochondria with fluorescent probes (LysoTracker and MitoTracker) in cortical neurons cultured 5 DIV and isolated from E14.5 WT or *Atat1* KO mouse embryos. Scale bars, 50 μm. (**I** to **L**). Histograms showing parameters of axonal transport of lysosomes to analyze average velocity (I), instantaneous velocity (J), run length (K), and pausing time (L) of mouse cortical neurons transfected with GFP or ATAT1-GFP, cultured 5 DIV, and isolated from E14.5 from WT or *Atat1* embryos. (**M**) Experimental setup for time-lapse recording of axonal transport in E15.5 cortical neurons isolated from E14.5 IUE mouse embryos and cultured 5 days in microfluidic device. N.S., not significant. (**N** to **Q**) Histograms showing parameters of axonal transport of lysosomes (LysoTracker) to analyze average velocity (N), instantaneous velocity (O), run length (P), and pausing time (Q) in mouse cortical neurons cultured 5 DIV from E15.5 embryos transfected with WT α-tubulin GFP (Tub-GFP) or acetylation mimic K40Q α-tubulin GFP (K40Q Tub-GFP) together with sh-Scramble (sh-Scr) or sh-Atat1. Description of graphical summaries here within are histograms of means ± SEM, while statistical analyses of (C to F) are two-tailed Mann-Whitney and (I, J, K, L, N, O, P, and Q) are Kruskal-Wallis test. Specifically [(C) $P < 0.0001$ and U = 17,455; (D) $P < 0.0001$ and U = 3044 and $P = 0.0002$ and U = 6372 for anterograde and retrograde, respectively; (E) $P < 0.0001$ and U = 20,972; (F) $P < 0.0001$ and U = 26,168; (I) $P < 0.0001$ and K = 54.03; (J) $P = 0.0033$ and K = 13.74 and $P < 0.0001$ and K = 36.45 for anterograde and retrograde, respectively; (K) $P < 0.0001$ and K = 38.29; (L) $P < 0.0001$ and K = 34.05; (N) $P < 0.0001$ and K = 31.88; (O) $P = 0.0006$ and K = 17.43 and $P = 0.0002$ and K = 20.19 for anterograde and retrograde, respectively; (P) $P < 0.0001$ and K = 22.29; and (Q) $P < 0.0001$ and K = 28.7).

(Fig. 1I and fig. S1, G, M, N, and R), anterograde and retrograde instantaneous velocities (Fig. 1J and fig. S1, H, M, N, and R), and run lengths (Fig. 1K and fig. S1, I, M, N, and R) of moving vesicles and mitochondria were reduced, while their pausing time were increased (Fig. 1L and fig. S1, J, M, N, and R). These modified vesicular parameters were associated with an impairment in the overall flux of organelles in *Atat1* KO mice (fig. S1, K, L, M, and N), likely arising from the reduced recruitment of motors onto MTs. Western blotting analyses revealed that lack of ATAT1 expression in newborn cortical neurons resulted in the absence of MT acetylation (fig. S1, O and P) without affecting the expression level of histone deacetylase 6 (HDAC6), the main α-tubulin deacetylase (fig. S1, O and Q). Expression of catalytically active ATAT1–green fluorescent protein (GFP) (*15*, *16*) in cortical neurons from E14.5 WT and *Atat1* KO embryos rescued the average velocity (Fig. 1I and fig. S1R), anterograde and retrograde instantaneous velocities (Fig. 1J and fig. S1R), run length (Fig. 1K and fig. S1R), and pausing time (Fig. 1L and fig. S1R) of lysosomes. To confirm that the defects in axonal transport upon down-regulation of *Atat1* arise from reduced α-tubulin acetylation, we coexpressed the acetyl mimic α-tubulin K40Q with shAtat1 (fig. S1S) in projection neurons of WT E14.5 embryos. We isolated the electroporated neurons 1 day after electroporation and cultured them 5 days in microfluidic devices (Fig. 1M). Our recordings showed that expression of α-tubulin K40Q rescued the average and instantaneous transport velocities of lysosomes (Fig. 1, N and O, and fig. S1X) and mitochondria (fig. S1, T, U, and Y), as well as their run lengths (Fig. 1P and fig. S1, V, X, and Y) and pausing time (Fig. 1Q and fig. S1, W, X, and Y) resulting from *Atat1* KD at E14.5.

We further examined whether the role of ATAT1 in axonal transport is conserved in vivo in *Drosophila melanogaster*. We assessed the transport of synaptotagmin-GFP vesicles in axons of third-instar larva motoneurons (Fig. 2, A and B, and movie S4) upon RNA interference (RNAi)–mediated KD of *Atat1/2* (the orthologs of mouse *Atat1* in *D. melanogaster*). Individual KDs of *Atat1* and *Atat2* were not compensated by expression of other α-tubulin acetylation regulators (fig. S2, A and B) and led to the reduction of average velocity (Fig. 2C and fig. S2C), anterograde and retrograde instantaneous velocities (Fig. 2D and fig. S2C), as well as run length (Fig. 2E and fig. S2C) of synaptotagmin-GFP vesicles, with associated increase of their pausing time (Fig. 2F and fig. S2C). The transport defects were not resulting from global protein aggregation along axons (fig. S2D) but were more likely associated with the decreased acetylation of MTs (Fig. 2, G and H). This was further supported by a genetic rescue of axonal transport upon concomitant depletion of the main α-tubulin deacetylase *Hdac6* (*17*) (fig. S2E) in motoneurons from individual KD of *Atat1* or *Atat2* larva (Fig. 2, C to F, and fig. S2C), where residual Atat activity can promote MT acetylation (Fig. 2, G and H). These data were also supported in the third-instar larvae fed for 30 min before recordings with 10% sucrose solution containing tubastatin (TBA), a specific inhibitor of HDAC6 (*18*), which rescued all measured axonal transport parameters (Fig. 2, I to L, and fig. S2F).

Impaired axonal transport in larvae or adult fly motoneurons leads to locomotor behavior deficits (*18*). We thus monitored the climbing index of adult flies as well as the crawling speed and peristaltic body-wave frequency of their larvae as functional readouts of single or combined KD of *Atat1/2* (*6*, *19*). These motoneuron-dependent activities were affected upon conditional KD of *Atat1/2* expression (Fig. 2, M to O) and were rescued by either a concomitant genetic depletion of *Hdac6* (Fig. 2, M to O) or inhibition of HDAC6 activity using TBA (Fig. 2, P and Q). The disruption of motor behaviors was most likely a consequence of fast axonal transport defects, since we did not observe morphological changes at the neuromuscular junctions' synapses (fig. S2, G and H) and the RNAi-mediated KD was restricted to motoneurons (see Materials and Methods). Together, these data support that ATAT1 promotes the acetylation of axonal MTs across vertebrate and invertebrate species and that acetylation of the MTs tracks is an important regulator of fast axonal transport.

We next assessed in a cell-free in vitro molecular transport assay how the reduction of K40 acetylation on MTs affects bidirectional axonal transport. For this purpose, purified vesicles were added to in vitro polymerized and polarity-marked MTs (to determine transport directionality), where 10% of rhodamine-labeled (acetylated) tubulin were mixed with either unacetylated tubulin from *Atat1* KO mouse brains or with endogenously acetylated tubulin from WT littermates (control) (Fig. 3, A and B, and movie S5). While MTs from *Atat1* KO mouse brains were lacking acetylation (*20*), they were not showing defects of polyglutamylation, glutamylation, tyrosination, or the abundance of Δ2 tubulin PTMs (Fig. 3C). In vitro transport analyses showed that vesicles' anterograde and retrograde instantaneous velocities (Fig. 3D and fig. S3A), together with their run lengths (Fig. 3E and fig. S3A), were reduced when vesicles were transported along *Atat1* KO brain-derived MTs as compared with acetylated MTs isolated from WT brains. These data were comparable to the one obtained in neurons in vitro and in vivo (Figs. 1, D and E, and 2, D and E) and further demonstrate that loss of α-tubulin K40 acetylation impairs MT-dependent transport.

## Atat1 is transported along MTs at the external surface of motile vesicles

Axons and dendrites are highly enriched in long-lived MTs, whose acetylation depends on ATAT1 distribution and activity. In vitro experiments have previously reported that recombinant ATAT1 undergoes slow and passive diffusion inside MT lumen (*12*). However, it remains unclear how ATAT1 reaches the MTs in living neurons; thus, we studied its axonal distribution in cultured cortical neurons isolated from E14.5 mice. Mouse cortical neurons were transfected with a combination of plasmids coding for brain-derived neurotrophic factor (BDNF)–mCherry and ATAT1-GFP and cultured 5 DIV. Analysis by superresolution microscopy revealed a punctate distribution of ATAT1 along axons, partially overlapping with the dense core vesicle marker BDNF, suggesting a possible vesicular enrichment of ATAT1 (Fig. 4A). The vesicular enrichment of ATAT1 was further confirmed in cultured human projection neurons derived from pluripotent stem cells, showing that expression of endogenous ATAT1 broadly codistributes with lysosomes (LAMP1 positive) and precursors of synaptic vesicles (SV2C and synaptophysin positives) along their axon (Fig. 4B).

To confirm the vesicular expression of ATAT1, we performed liquid chromatography–tandem mass spectrometry (LC-MS/MS) on vesicular extracts isolated from the cortex of newborn mice. The analysis of the vesicular enriched fraction detected 3648 proteins whose overlap with published vesicular proteomes was, in average, 75% (*21*–*23*) (Fig. 4C). These analyses showed that ATAT1, but not HDAC6, is detected together with kinesins and dyneins in a mid-range fraction of the vesicular proteomic content (Fig. 4D and table S1). Western blot analysis of the subcellular fractions obtained from

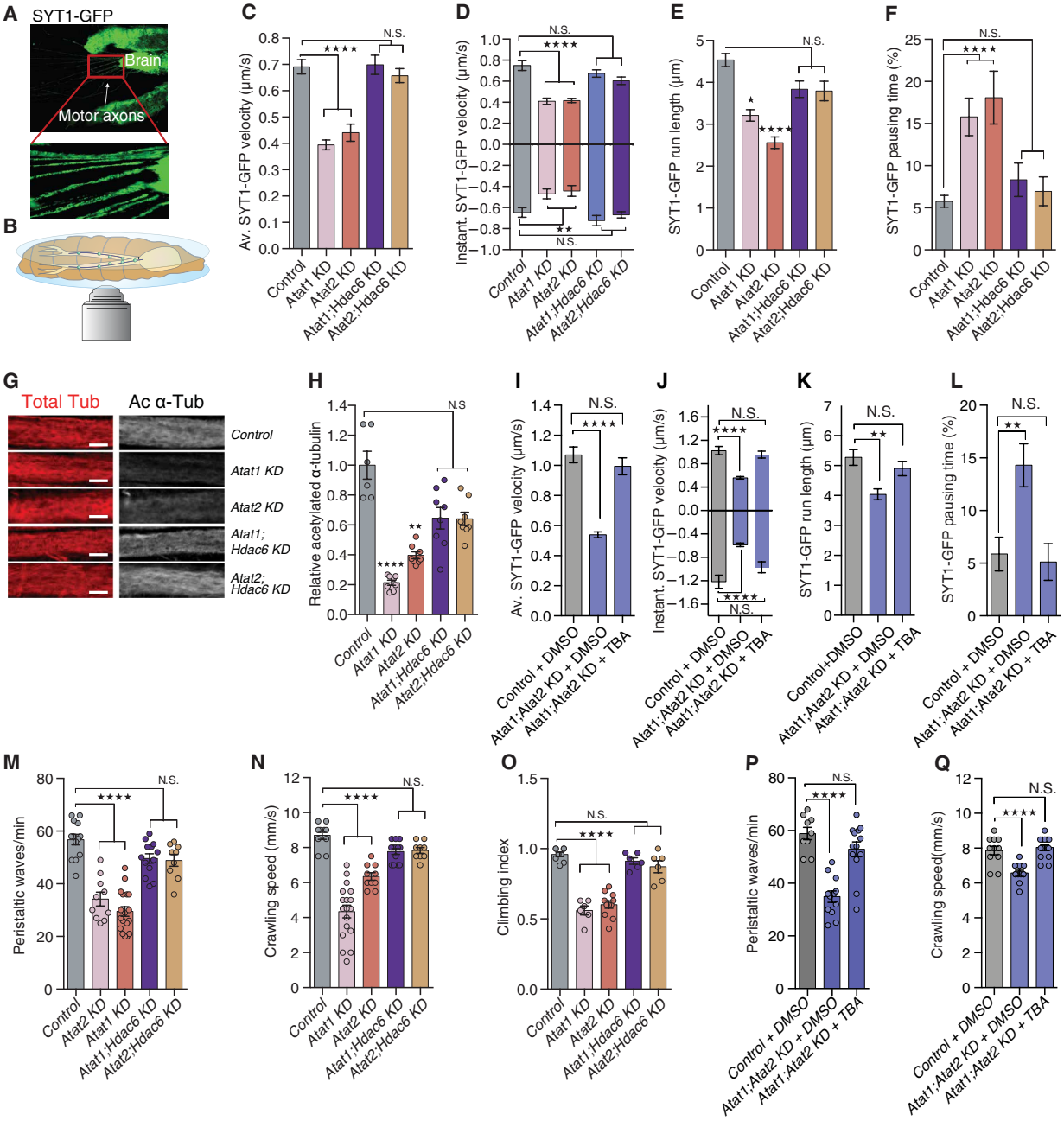


**Fig. 2. Depletion of Atat1 prevents acetylation of α-tubulin and interferes with fast axonal transport of organelles in vivo.** (**A** and **B**) In vivo live-imaging setup used to record axonal transport of synaptotagmin-GFP (SYT1-GFP in green) in *D. melanogaster* third-instar larvae expressing UAS:RNAi under a motoneuron-specific driver (D42:GAL4) to analyze average velocity (**C**), instantaneous velocity (**D**), run length (**E**), and pausing time (**F**). (**G** and **H**). Analyses of immunolabeled motoneurons from third-instar larvae to detect total α-tubulin (Tot α-tub) and acetylated α-tubulin (Ac α-tub). Scale bars, 10 µm. (**I** to **L**) Axonal transport recording in *Atat1;Atat2* KD third-instar larvae fed for 30 min before recording with 10% sucrose with 1 mM TBA or dimethyl sulfoxide (DMSO) to measure SYT1-GFP average velocity (I), instantaneous velocity (J), run length (K), and pausing time (L). (**M** and **N**) Larva peristaltic movements and crawling speed in third-instar larvae expressing RNAi under a motoneuron-specific driver (D42:GAL4). (**O**) Climbing index in adult flies expressing RNAi under a motor neuron-specific driver. (**P** and **Q**) Larva peristaltic movements and crawling speed in third-instar larvae expressing RNAi under a motoneuron-specific driver (D42:GAL4) or in control and *Atat1;Atat2* KD larva prefed for 30 min with 10% sucrose with 1 mM TBA or DMSO. Description of graphical summaries here within are histograms of means ± SEM, while statistical analyses of (C, D, E, F, H, I, J, K, and L) are Kruskal-Wallis and (M to Q) is one-way analysis of variance (ANOVA). Specifically [(C) $P < 0.0001$ and K = 60.10; (D) $P < 0.0001$ and K = 65.80 and $P < 0.0001$ and K = 76.02 for anterograde and retrograde respectively; (E) $P < 0.0001$ and K = 25.39; (F) $P < 0.0001$ and K = 9.6; H, $P < 0.0001$ and K = 30.09; (I) $P < 0.0001$ and K = 121.1; (J) $P < 0.0001$ and K = 62.57 and $P < 0.0001$ and K = 50.34 for anterograde and retrograde, respectively; (K) $P < 0.0001$ and K = 24.3; (L) $P < 0.0001$ and K = 12.96, M, $P < 0.0001$ and $F(4, 58) = 34.55$; (N) $P < 0.0001$ and $F(4, 55) = 40.83$; (O) $P < 0.0001$ and $F(4, 33) = 45.61$; (P) $P < 0.0001$ and $F(7, 71) = 27.29$; and (Q) $P < 0.0001$ and $F(7, 83) = 47.65$]. In addition, post hoc multiple comparisons for (C, D, E, F, I, J, K, L, and H) Dunn's tests, for (M to Q) is Dunnett's test and are $^*P < 0.05$, $^{**}P < 0.01$, $^{***}P < 0.001$, and $^{****}P < 0.0001$. The total number of samples analyzed were as follows: (C to F) 110 to 276 vesicle tracks from 7 to 12 larvae per group; (H) 6 to 8 larvae per group; (I to L) 112 to 161 vesicle tracks from at 6 to 8 larvae per group; (M and N) 9 to 18 larvae per group; (O) 6 to 11 assays per group; and (P and Q) 8 to 9 larvae per group.

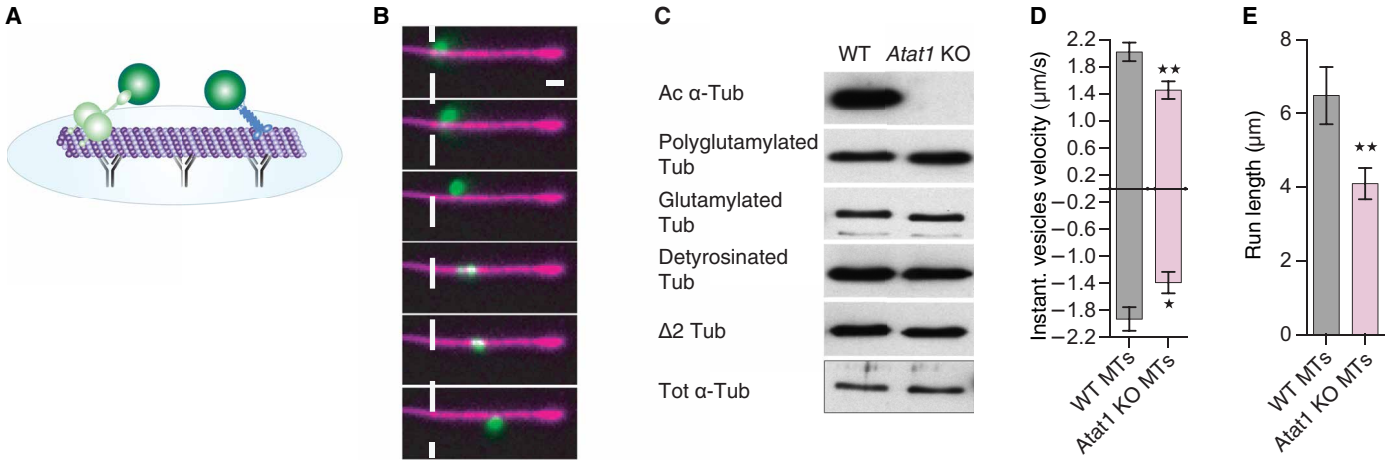


**Fig. 3. Vesicle transport is reduced on nonacetylated MTs in vitro.** (**A**) Scheme representing the experimental setup to study in vitro transport and acetylation assays. (**B**) Total internal reflection fluorescence (TIRF) image series of rhodamine-labeled MTs (10%, purple) with a transported DIO (green)–labeled vesicle from mouse brains. Scale bar, 2 μm; presented frames are in a 400-ms interval. (**C**) Western blott (WB) analyses to detect acetylated, glutamylated, polyglutamylated detyrosinated, Δ2, or total α-tubulin (Tub) in cortical brain extracts of WT or *Atat1* KO adult mice. (**D** and **E**) In vitro transport assay of vesicles purified from WT mice with nonacetylated α-tubulin from *Atat1* KO mouse brain or endogenously acetylated α-tubulin from WT mice. Histogram of anterograde and retrograde instantaneous velocities (D) and run length (E) of moving vesicles. Description of graphical summaries here within are histograms of means ± SEM, statistical analyses of (D) and (E) are two-tailed *t* test. Specifically [(D) $P = 0.0299$ and t, df(2,273,32) and $P = 0.0054$ and t, df(2,971,34) for retrograde and anterograde, respectively; and (E) $P = 0.0086$ and U = 50]. The total number of samples analyzed were as follows: (D and E) 16 to 20 vesicles from three WT or *Atat1* KO mice.

protein extract of newborn mouse brains confirmed the selective enrichment of ATAT1 in the vesicular fraction (P3), contrasting with the predominant cytosolic distribution of HDAC6 (S3) (Fig. 4E). Moreover, time-lapse recordings showed that ATAT1-GFP clusters move bidirectionally together with lysosomes (LysoTracker, Fig. 4F) and dense core vesicles (BDNF-mCherry, Fig. 4F) at velocities that are consistent with axonal transport in transfected cortical projection neurons (Fig. 4, G and H, and movie S6) (*24*). These data demonstrate that ATAT1 is enriched in the vesicular fraction and that it is transported along axons by motile vesicles.

ATAT1 binds to clathrin-coated vesicles via an AP2 binding domain (amino acids 307 to 387) (*25*), which is only conserved by its isoforms 1 and 2 (Fig. 4I). Our LC-MS/MS analysis did not detect peptides corresponding to the AP2 binding domain of ATAT1 in purified vesicles extracts (fig. S4A), and Western blott (WB) performed on mice cortical brain extracts only detected the presence of ATAT1 isoforms 3 and 4 (Fig. 4E), suggesting that the AP2 binding domain is not required for the recruitment of ATAT1 to motile vesicles.

To identify ATAT1's vesicle binding domain, we engineered distinct truncated ATAT1 forms by deleting amino acid sequences between the minimal catalytic domain of ATAT1 (amino acids 1 to 196) and the C-terminal part of isoform 4 (amino acids 1 to 333) (Fig. 4I). These constructs were next used to transfect human embryonic kidney (HEK) 293 cells and analyzed for their subcellular localization by WB (Fig. 4, J and K). ATAT1 isoform 4 and its amino acid 1 to 286 truncation were enriched in vesicles [vesicles (P3)/cytosol fraction ratio (S3) > 1], while the other truncated forms (1 to 242 and 1 to 196) preferentially localized in the cytosol (P3/S3 < 1) (Fig. 4K). Moreover, expression of the vesicular-enriched ATAT1 isoforms was more efficiently raising the level of α-tubulin acetylation when expressed in HeLa S3 cells as compared to the others (Fig. 4, L and M). Together, these data suggest that the amino acid sequence of ATAT1 comprised between amino acids 242 to 333 is required for both its vesicular enrichment and efficient α-tubulin acetylation.

To decipher whether ATAT1 is encapsulated within the intravesicular lumen and/or associated with the extravesicular membrane, we performed a mild proteinase K digestion to remove protein anchored at the external surface of vesicles (*26*). The treatment led to a dose-dependent reduction of ATAT1 and dynein intermediate chain (DIC) without altering levels of the intravesicular protein α-synuclein (Fig. 4N) (*26*). Together, these data suggest that ATAT1 is enriched at the cytosolic side of moving vesicles, from where it may be released in vicinity of MTs to promote α-tubulin acetylation and modulate axonal transport.

## The vesicular pool of Atat1 controls axonal transport by promoting acetylation of MTs

We first performed LC-MS/MS on vesicular extracts isolated from the cortex of newborn WT or *Atat1* KO mice to check whether loss of Atat1 interferes with axonal transport by altering the vesicular proteome. The analysis revealed that, from 44 differentially detected proteins (fig. S5A and table S2), none of the 29 molecular motor proteins (fig. S5B and table S3) nor the 16 glycolytic enzymes (fig. S5C and table S4) were significantly affected by lack of Atat1 expression. Moreover, gene ontology (GO) data analysis of the differentially detected proteins did not reveal significantly enriched processes, function, or cellular component upon Atat1 loss in vesicular extracts. Since we did not detect any differences of the *Atat1* KO vesicular proteome that can explain the reduction of MT acetylation, we hypothesized that Atat1-enriched vesicle displacement on MTs might be required for their acetylation. To test this hypothesis, we cultured mouse cortical neurons with the cytoplasmic dynein inhibitor ciliobrevin D (20 μM) (*27*) to disrupt axonal transport of vesicles. This led to a mild reduction (33%) of MT acetylation in the soma of the neurons (Fig. 5, A and B) and a severe reduction (67%)

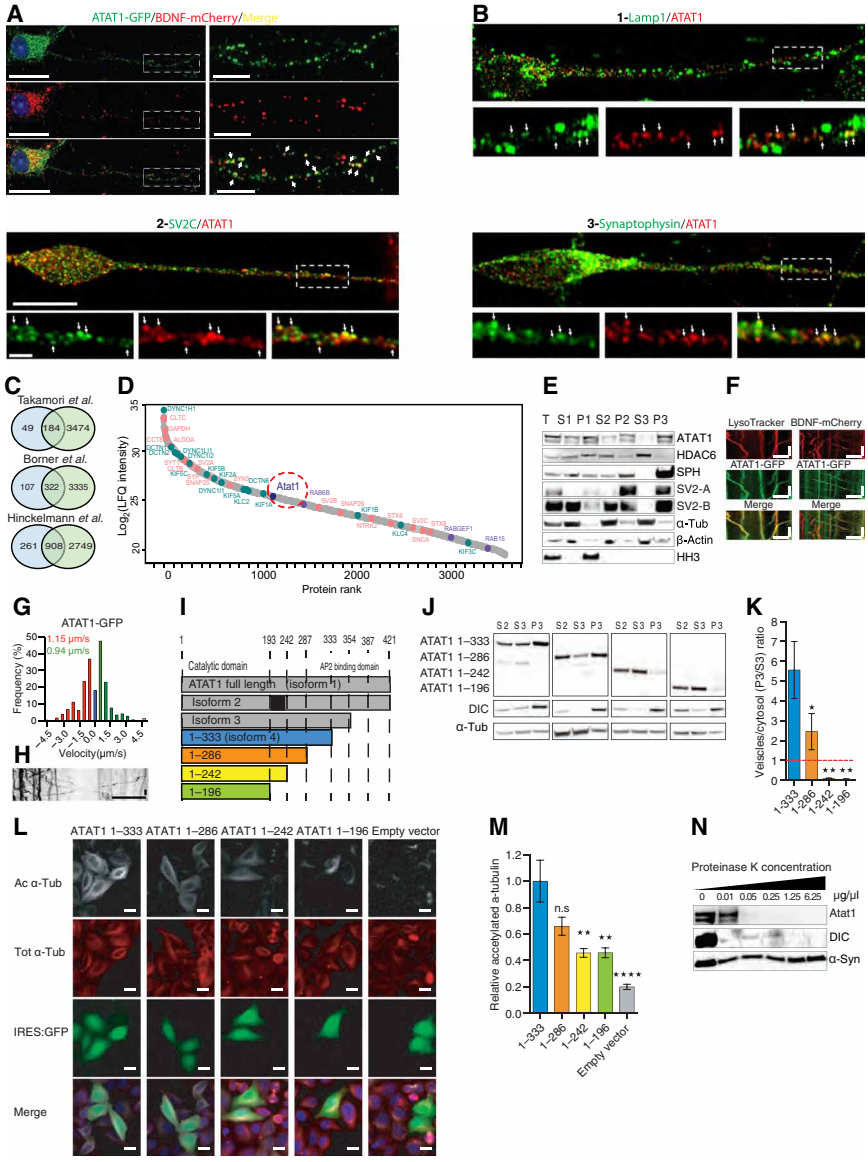


**Fig. 4. ATAT1 is a vesicular-enriched protein that localizes on the cytosolic side of the vesicular membrane.** (**A**) Superresolution image of a transfected E14.5 cortical neuron-cultured 5 DIV and labeled for 4′ 6-diamidino-2-phenylindole (DAPI) (blue), ATAT1-GFP (green), and BDNF-mCherry (red). Scale bar is 20 μm for the original image and 5 μm for the magnified area. (**B**) Superresolution imagine of day 36 human projecting neurons derived from hIPSCs and immunostained for ATAT1 along with 1, Lamp1; 2, SV2C; and 3, synaptophysin. Arrowheads indicate codistribution of markers. Scale bar is 10 and 1 μm for the original image and magnified area, respectively. (**C**) Venn diagrams of vesicular content identified by LC-MS/MS in this work and previous publications. (**D**) LC-MS/MS of vesicle fraction isolated from newborn mouse brain cortices, proteins were ranked by intensity and plotted according to their relative abundance (gray spots). Atat1 (pink) detection among proteins previously identified as vesicular components (purple) and molecular motors (green) ($n = 3$, graph represent the mean intensity value). (**E**) Subcellular fractionation (T, total; S1, postnuclear; P1, nuclear; S2, cytosol and vesicles; P2, larges membranes; S3, cytosol; and P3, vesicles) of mouse brain cortex showing predominant vesicular enrichment of Atat1, immunostained with antibodies (Table 1) against ATAT1 (isoform 3 and 4 corresponding to 37 and 30 kDa), histone deacetylase 6 (HDAC6), synaptophysin (SPH), synaptic vesicle glycoprotein 2A/B (SV2A/B), β-actin, α-tubulin (α-tub), and histone H3 (HH3) antibodies. (**F**) Kymographs of ATAT1-GFP and LysoTracker or BDNF-mCherry in E14.5 cortical neurons axons cultured 5 DIV, showing partial cotransport of Atat1 and lysosomes or BDNF-mCherry. Scale bars, 10 μm ($x$) and 20 s ($y$). (**G** and **H**) Bin distribution and kymograph of ATAT1-GFP transport velocities in transfected E14.5 cortical neurons cultured 5 DIV ($n = 5$; $n$ for anterograde =143, retrograde = 179). Scale bars, 10 μm ($x$) and 20 s ($y$). (**I**) Schematic representation of truncated ATAT1 isoform four constructs. (**J** and **K**) Subcellular fractions of cultured HEK293 cells were analyzed using WB to detect ATAT1 truncated forms (J), vesicles/cytosol (P3/S3) ratios were quantified to identify vesicular enrichment (ratio > 1) of the various truncated ATAT1 forms (K). (**L** and **M**) Transfected HeLa cells with ATAT1:IRES-GFP truncated constructs were immunolabeled for acetylated α-tubulin (Ac α-tub, gray), total α-tubulin (Tot α-tub, red), and DAPI (blue) and analyzed for their relative acetylated α-tubulin levels [Ac α-tub/Tot α-tub ratio, controls are set to 1, (M)]. Scale bar, 10 μm. (**N**) WB analysis of cerebral cortex vesicles subjected to proteinase-K digestion. Intravesicular α-synuclein is digestion resistant, while the outer vesicular membrane motor protein DIC as well as Atat1 were digested in an enzymatic concentration–dependent manner. Description of graphical summaries here within are histograms of means ± SEM; statistical analyses of (K) is one-way ANOVA and (M) is Kruskal-Wallis. Specifically [(K) $P = 0.0018$ and $F(3,12) = 17.29$; (M) $P < 0.0001$ and K = 83.16]. In addition, post hoc multiple comparisons are Holm-Sidak's tests (K), and Dunn's test (M); *$P < 0.05$, **$P < 0.01$, and ****$P < 0.0001$. The total number of samples analyzed were four independent HEK293 cultures (K) and four independent HeLa cultures (M) per ATAT1 truncation construct.

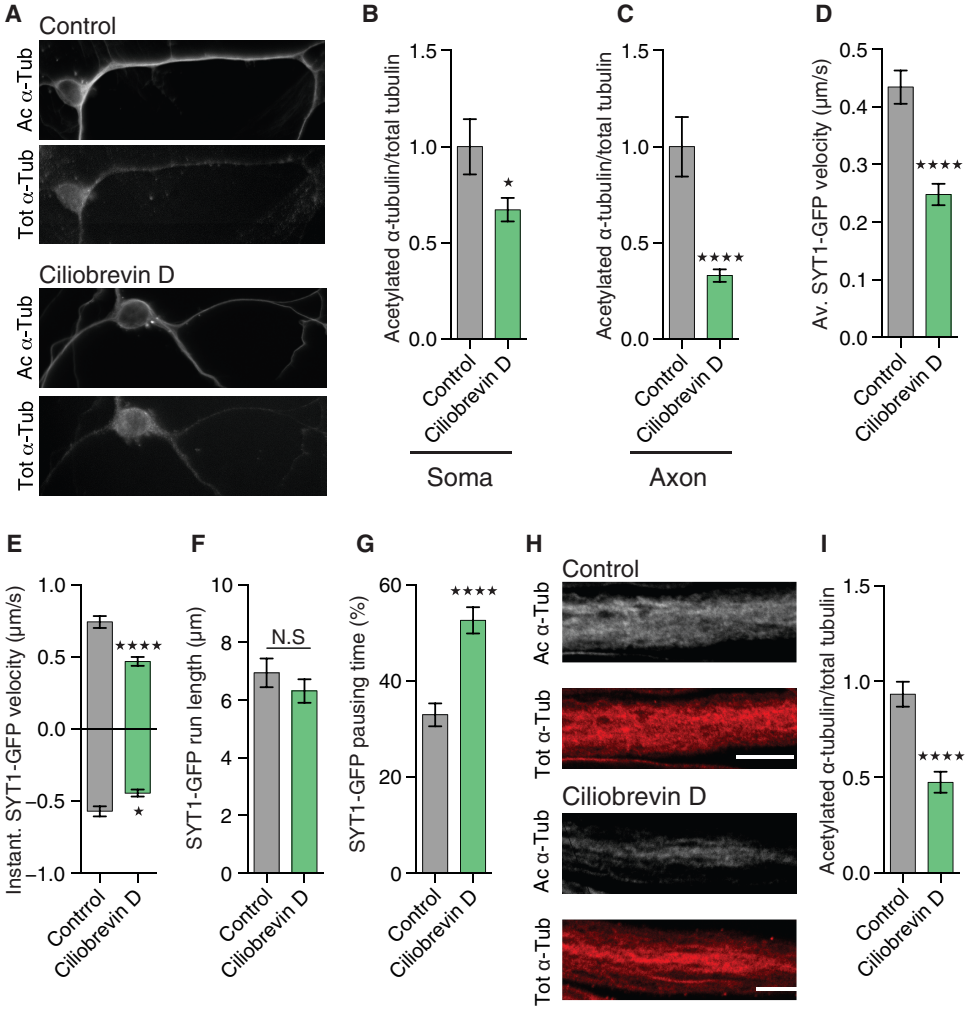


**Fig. 5. Ciliobrevin disrupts α-tubulin acetylation and axonal transport in vitro and in vivo.** (**A** to **C**) Immunolabeled cortical neurons from E14.5 mice embryos treated with 20 μM of ciliobrevin D of control buffer 1 hour before fixation, showing total α-tubulin (Tot α-tub) and acetylated α-tubulin (Ac α-tub) in the soma (B) or distal axons (C) of the neurons. Scale bar, 10 μm. (**D** to **G**) Axonal transport in motoneurons from synaptotagmin-GFP *D. melanogaster* third-instar larvae fed during 2 hours with 800 μM of DMSO (control) or ciliobrevin D before the analysis of average SYT1-GFP vesicle velocity (D), instantaneous velocity (E), run length (F), and pausing time (G). (**H** and **I**) Immunolabeled motoneurons from third-instar larvae fed with 800 μM of ciliobrevin D 2 hours before sacrifice, showing total α-tubulin (Tot α-tub) and acetylated α-tubulin (Ac α-tub). Scale bar,10 μm. Description of graphical summaries here within are histograms of means ± SEM; statistical analyses of (B) and (C) are two-tailed *t* test, while those of (D) to (G) are two-tailed Mann-Whitney. Specifically, [(B) $P = 0.0419$ and t, $df_{(2.051,\ 58)}$; (C) $P < 0.0001$ and U = 699; (D) $P < 0.0001$ and U = 23,096; (E) $P = 0.0005$ and U = 3857 and $P = 0.0209$ and U = 3,293 for anterograde and retrograde, respectively; (F) $P = 0.7385$ and U = 37,999; (G) $P < 0.0001$ U = 28,877; and (I) $P < 0.0001$ and U = 336). The total number of samples analyzed was (B and C) 29 to 50 neurons from four embryos; (D to G) = 116 to 279 SYT1-GFP tracks from 6 to 8 larvae per group; and (I) 37 to 49 neurons from 8 to 10 larvae. *$P < 0.05$ and ****$P < 0.0001$.

of acetylation of distal axonal MTs (Fig. 5, A and C) as a result of a reduction of axonal transport (Fig. 5D and fig. S6L). At this concentration, ciliobrevin D blocks both retrograde and anterograde transports (*27*); we thus specifically reduced retrograde transport by knocking down Lis1 in mouse cortical neurons (fig. S6, A to H). This led to a reduction of MT acetylation in the axon but not in the soma of these neurons (fig. S6, I to K). Moreover, feeding *Drosophila* third-instar larvae with ciliobrevin D (800 μM) disrupted anterograde and retrograde axonal transport (Fig. 5, E to G, and fig. S6A) and decreased MT acetylation (Fig. 5, H and I) in motoneurons in vivo to a level comparable with the one observed upon expression of *Atat1/2* RNAi (Fig. 2, G and H). These results show that disrupting axonal transport impairs MT acetylation, a defect that correlates with a lack of mobility of Atat1-enriched vesicles along the axonal MTs.

To test whether the vesicular pool of Atat1 promotes the acetylation of α-tubulin in MTs, we isolated subcellular fractions from newborn mouse cortices and then assessed their ability to promote the acetylation of nonacetylated MTs isolated from HeLa cells (*8*), compared with endogenously acetylated bovine brain MTs (control) (Fig. 6A). We observed that most of the MT acetyltransferase activity was detected in the vesicular fraction (Fig. 6B), an activity that was lost in either vesicles isolated from *Atat1* KO mice or vesicles incubated without acetyl–coenzyme A (CoA), the acetyl group donor for Atat1-dependent MT acetylation (Fig. 6, C to E) (*15*). Moreover, the vesicular fraction was able to promote the acetylation of MTs over several hours in vitro, as suggested by the strong reduction of CoA release upon incubation with vesicles from *Atat1* KO mice, as compared to WT control (Fig. 6F). These findings suggest that the

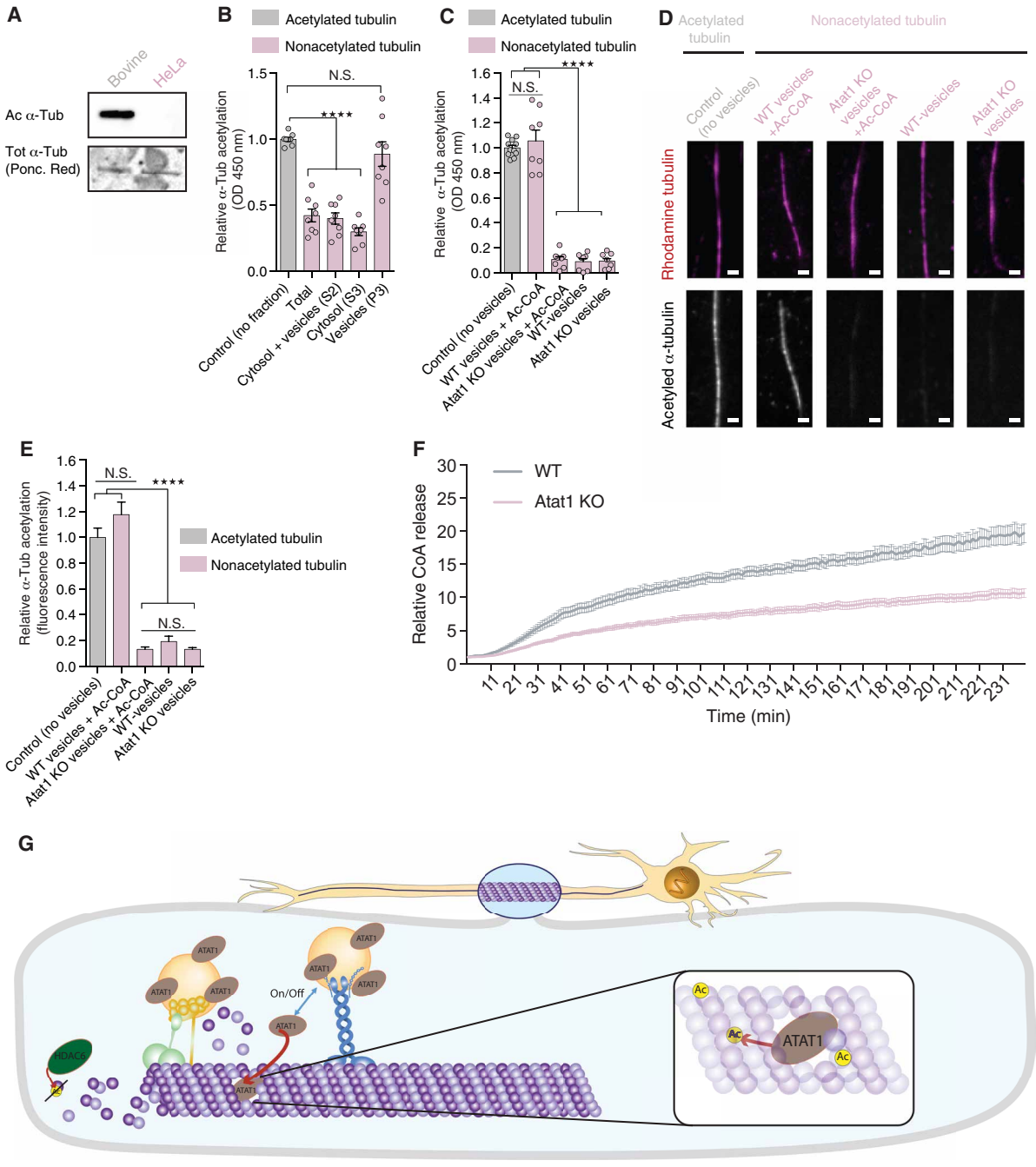


**Fig. 6. Vesicles predominantly promote α-tubulin acetylation via ATAT1.** (**A**) WB analysis of purified tubulin from bovine brain and HeLa cells, showing acetylated α-tubulin (Ac α-tub). Ponceau red identified total α-tubulin (Tot α-tub) on corresponding extracts. (**B** and **C**) In vitro enzyme-linked immunosorbent assay (ELISA)–based α-tubulin acetylation assay of polymerized nonacetylated MTs from HeLa cells; incubated with subcellular fraction (B); or with vesicular fractions isolated from WT or *Atat1 KO* mouse brain cortices with acetyl-CoA or vehicle (C). Purified bovine endogenously acetylated MTs served as control. (**D** and **E**) α-Tubulin acetylation assay of in vitro polymerized nonacetylated MTs from HeLa cells incubated with vesicular fractions (P3) isolated from WT or *Atat1* KO mouse brain cortices and acetyl-CoA or vehicle. Purified bovine endogenously acetylated MTs served as control. Fluorescent signal was measured for total α-tubulin by using rhodamine dye and for acetylated α-tubulin by immunolabeling. Scale bar, 2 μm. (**F**) In vitro α-tubulin acetylation assay based on CoA release from acetyl-CoA by incubating vesicles from WT or *Atat1* KO mice with polymerized nonacetylated MTs from HeLa cells. (**G**) Scheme depicting the axonal transport (anterograde and retrograde) of vesicles enriched in ATAT1 at their external surface. The proper acetylation of MTs is linked to the axonal transport of these vesicles and we propose that axonal transport transiently disrupt the MT lattice by creating transient openings through which ATAT1 relocates intralumenally to promote K40 α-tubulin acetylation. Description of graphical summaries here within are histograms of means ± SEM, while statistical analyses of (B and C) are one-way ANOVA; (D) is Kruskal-Wallis and (F) is two-way ANOVA. Specifically [(B) $P < 0.0001$ and $F_{(4,35)}=35.56$; (C) $P < 0.0001$ and $F_{(4,38)}=158.3$; (E) $P < 0.0001$ and K = 120.8; (F) $P < 0.0001$ and $F_{(1,3360)} = 8113$) In addition, post hoc multiple comparisons are Sidak's tests (B and C): Dunn's test (D); ****$P < 0.0001$. The total number of samples analyzed were as follows: (B and C) eight subcellular brain cortical fractions from eight newborn mice; (E) = 29 to 46 MTs, (F) 240 sample points (1/min) of purified vesicles from three WT and three *Atat1* KO mouse brain cortices.

**Table 1. List of antibodies and their dilution used for ELISA assays, immunostainings, and/or Western blottings.**

| Protein | Company | Cat no. | WB | IF | ELISA |
|---|---|---|---|---|---|
| α-Tubulin | Sigma-Aldrich | T9026 | 1:5000 | | 1:2,000 |
| α-Tubulin* | DSHB | 12G10 | 1:500 | | |
| α/β-Tubulin | Cytoskeleton | ATN02-A | | 1:150 | |
| Acetylated α-tubulin | Sigma-Aldrich | T7451 | 1:15,000 | 1:15,000 | |
| Polyglutamylated tubulin | AdipoGen | AG-25B-0030 | 1:10,000 | | |
| Glutamylated tubulin | AdipoGen | AG-20B-0020 | 1:10,000 | | |
| Detyrosinated tubulin | Millipore | AB3201 | 1:1,000 | | |
| Δ2-Tubulin | Millipore | AB3203 | 1:2,000 | | |
| Lis1 | Santa Cruz | Sc-393320 | 1:100 | 1:100 | |
| ATAT1 | Sigma-Aldrich | HPA046816 | 1:2000 | 1:120 | |
| GAPDH | Millipore | MAB374 | 1:300 | | |
| LAMP1 | Abcam | Ab25630 | | 1:20 | |
| Synaptophysin | Synaptic Systems | 101 004 | | 1:1000 | |
| SV2C | Synaptic Systems | 119 204 | | 1:500 | |
| GFP | Origene | TP401 | 1:5000 | | |
| GFP | Abcam | Ab6673 | | 1:1000 | |
| β-Actin | Sigma-Aldrich | A3853 | 1:20,000 | | |
| HDAC6 | Santa Cruz Biotechnology | sc-5258 | 1:200 | | |
| GFP | Molecular Probes | A11122 | 1:1000 | | |
| ATAT1 | Maxence Nachury | | 1:1000 | | |
| CSP** (cystein-string protein) | DSHB | DCSP-2 (D6D) | | 1:10 | |
| HRP | Sigma-Aldrich | P97899 | | 1:1,000 | |
| FLAG | Sigma-Aldrich | F3165 | 1:1,000 | | |
| Synaptophysin | Sigma-Aldrich | s5768 | 1:1,000 | | |
| Histone H3 | cell signaling | 9715 | 1:5,000 | | |
| Synuclein | Abcam | ab51252 | 1:5,000 | | |
| DIC | Millipore | MAB1618 | 1:500 | | |
| SV2*** | DSHB | AB 2315387 | 1:100 | | |
| β-Tubulin | cell signaling | 2146 | | 1:100 | |
| Goat anti mouse | Jackson ImmunoResearch Labs | 115–035-003 | 1:10,000 | 1:200 | 1:5,000 |
| Goat anti rabbit | Jackson ImmunoResearch Labs | 111-035-003 | 1:10,000 | 1:200 | |
| Donkey anti goat | Jackson ImmunoResearch Labs | 705-035-003 | 1:10,000 | | |

*12G10 anti–α-tubulin was deposited to the DSHB by J. Frankel/E.M. Nelsen (DSHB hybridoma product 12G10 anti–α-tubulin). **DCSP-2 (6D6) was deposited to the DSHB by S. Benzer [DSHB hybridoma product DCSP-2 (6D6)]. ***SV2 was deposited to the DSHB by K.M. Buckley (DSHB hybridoma product SV2).

pool of vesicular Atat1 provides an enzymatic activity that promotes MT acetylation and thereby fast axonal transport (Fig. 6G).

## DISCUSSION

Here, we show that loss of *Atat1*(/2), thereby MT acetylation, impairs bidirectional axonal transport in mouse cortical neurons in culture or in organotypic slice as well as in fly larva motoneurons in vivo, ultimately resulting in locomotor defects in adult flies. Our work revealed the existence of a large pool of functional Atat1 at the external surface of different types of motile vesicles, including lysosomes and precursors of synaptic vesicles. Moreover, blocking MT-dependent transport impaired α-tubulin acetylation, further suggesting that Atat1-enriched vesicles have to be transported along MT to promote α-tubulin acetylation. Treatment with high concentration of ciliobrevin D (that blocks both retrograde and anterograde transport;

Fig. 5E) or expression of shLis1 (that blocks retrograde transport; fig. S6E) significantly reduced MT acetylation in the axon, while only ciliobrevin D treatment did so in the soma. This suggests a possible predominant role for the anterograde transport of Atat1-enriched vesicles to promote α-tubulin acetylation in the soma, a hypothesis whose validation would require additional experiments.

Increasing MT acetylation has been shown to compensate for axonal transport defects in fly, mouse, and human models (*6*, *16*). However, the role of Atat1 in axonal transport has been debated, since loss of Atat1/MEC17 expression impairs axonal transport in *Caenorhabditis elegans* neurons (*28*) but not in hippocampal and dorsal root ganglia neurons from adult mice (*29*). This apparent discrepancy may reflect different contributions of Atat1, thereby MT acetylation to axonal transport in distinct neuronal populations. It is also unexpected that, while acute deletion of *Atat1* impairs MT acetylation, neuronal migration, and axon branching in the developing rodent cortex (*30*), *Atat1* KO mice only show mild neurological abnormalities such as increased anxiety and impairments in mechanosensation (*14*, *29*). Such discrepancy may reflect a stronger requirement for Atat1 during development and early life, as suggested by its decreasing expression after birth in the cerebral cortex of both mice (*30*) and humans (*31*) (figure S7, 2018 Allen Institute for Cell Science. BrainSpan Atlas of the Developing Human Brain. Available from: brainspan.org/rnaseq/search/index.html).

Recent work performed in vitro has suggested that ATAT1 diffuses in the lumen of MTs where it induces acetylation of α-tubulin K40 (*12*). While the mode of intraluminal relocation of ATAT1 remains controversial (*11*, *12*), we now suggest that motile vesicles bring ATAT1 in close vicinity to MTs, which is in accord with the detection of ATAT1 at the surface of MTs by electronic scanning microscopy (*9*). Supposing that molecular transport triggers transient MT lattice deformations (*32*, *33*) and disruption (*34*), one can postulate that locally released vesicular ATAT1 could reach the MT lumen to acetylates α-tubulin K40 in vivo via these dynamic lateral openings (*35*).

The results of our work, together with the observation that vesicular glyceraldehyde-3-phosphate dehydrogenase (GAPDH) activity contributes to local generation of adenosine triphosphate (ATP) for fast-moving vesicles (*24*), show that vesicles have on-board enzymatic machinery that can act locally and modulate their own transport by changing their molecular environment. Our work suggests, in particular, that in neurons, vesicle-associated enzymes can locally modify MT tracks, thus optimizing axonal transport. Reduced acetylation of MTs also affect their flexibility and thus resistance to physical breakage after repeated mechanical stress (*10*, *36*), and loss of Atat1/MEC17 in *C. elegans* leads to MT instability and axonal degeneration (*28*). Therefore, it would be interesting to test whether a reduced vesicular axonal transport, as observed in neurodegenerative diseases (*37*), might contribute to the neurodegeneration process via curtailing the acetylation of α-tubulin, hence leading to a global weakening and breakage of axonal MTs.

## MATERIALS AND METHODS

### Mice

Mice were euthanized and brain cortices were harvested either at P0 to P2 for biochemical analysis or E14.5 for preparation of cortical neuronal cultures. *Atat1*$^{+/-}$ mice were used to obtain WT and KO mice (*14*). Mice were maintained with access to food and water ad libitum and kept at a constant temperature (19° to 22°C) and humidity (40 to 50%) on a 12:12-hour light/dark cycle according to the guidelines of the Belgian Ministry of Agriculture and in agreement with the European Community Laboratory Animal Care and Use Regulations (86/609/CEE, Journal Officiel des Communautés Européennes L358, 18 December 1986). All experimental procedures were performed in strict accordance with the recommendations of the European Community (86/609/EEC) for care and use of laboratory animals under the supervision of authorized investigators.

### *D. melanogaster* maintenance and lines

Flies were kept at a 25°C incubator with a 12-hour light and dark cycle. Crosses were performed at 25°C, first-instar larvae were transferred to a 29°C incubator until use. For axonal transport, behavioral experiments and immunolabeling D42-Gal4-UAS: Syt1-GFP or D42-Gal4 virgin females were crossed with upstream activation sequence (UAS)–RNAi carrying lines. For quantitative polymerase chain reaction (qPCR) analysis, elav-Gal4 females were crossed with UAS-RNAi males. All RNAi inserts sequences were validated by Sanger sequencing.

Drosophila lines were acquired from the Vienna Drosophila Resource Center (VDRC) and the Bloomington Drosophila Stock Center (BDSC). UAS-*Syt1:GFP* (BDSC 6925), UAS-RNAi *Atat1* (VDRC CG3967), UAS-RNAi *Atat2* (VDRC CG17003), UAS-RNAi *Hdac6* (BDSC 51181), and UAS-RNAi *Zpg* (VDRC CG10125) were used as control. Elav-Gal4 (BDSC 458) or D42-Gal4 (BDSC 8816) flies were used for specific activation of a UAS sequence in postmitotic neurons or motor neurons, respectively. All RNAi insert sequences were validated by Sanger sequencing.

### Constructs

BDNF-mCherry was previously used in (*24*) and ATAT1-GFP (27099), pCALNL-DsRed (13769), and pEGFP α-tubulin K40Q (105302) were purchased from Addgene (www.addgene.org/). pEGFP-Tub was obtained from Clontech (www.takarabio.com/). pCAG mEmerald-LAMP1 and pCAG mito-DsRED were provided by F. Polleux (Columbia University, New York, USA), and pCAG-iCreERT2 was provided by A. Tye (NIMR, UK). pCX-Cre plasmid was designed and provided by X. Morin (Institut de Biologie de l'Ecole Normale Superieure IBENS, France). ATAT1 truncation constructs, FLAG-ATAT1(amino acids 1 to 333), FLAG-ATAT1(amino acids 1 to 286), FLAG-ATAT1(amino acids 1 to 242), and FLAG-ATAT1(amino acids 1 to 196) were synthesized as gBlocks and inserted to a pCIG2 vector. The *Atat1* short hairpin RNA (shRNA) sequence was 5′-GCAGCAAATCATGACTATTGT-3′ (*30*). *Atat1* sequence was inserted in pBS/U6-ploxPneo plasmid (provided by X. Coumoul). Lis1 shRNA sequence was 5′-GAGATGAACTA-AATCGAGCTA-3′ (*38*) and was subcloned in pCA-b-EGFPm5 silencer 3, a gift from M. Vermeren (King's College London, UK). All construct sequences were verified by Sanger sequencing.

### Cell lines culture, transfections, and drug treatment

Mouse neuroblastoma N2A cells were cultured in Dulbecco's modified Eagle's medium (DMEM) (Gibco) supplemented with 10% fetal calf serum at 37°C with 5% $CO_2$. To test shAtat1 efficiency, we treated N2A cells with 4OHT (1 μM) 24 and 48 hours after lipofection with Lipofectamine 2000 (Invitrogen), and cell lysis or fixation was performed 48 hours after the first treatment with 4OHT.

### Neuronal cell culture

E14.5 mouse brain cortices were dissected and mechanically dissociated in Hanks' balanced salt solution (HBSS) (Sigma-Aldrich, H6648)

supplemented with 1.5% glucose. Cells were cultured at a confluence of ~70% with Neurobasal Medium (Gibco, Invitrogen, 21103049) supplemented with 2% B27 (Gibco, Invitrogen, 17504044), 1% penicillin/streptomycin (Gibco, Invitrogen, 15140122), and 1% GlutaMAX (Gibco, Invitrogen, 35050061) at 37°C. Nucleofections of E14.5 cortical neurons were performed using Mouse Neuron Nucleofector Kit (VPG-1001, Lonza) according to the manufacturer's protocol.

### Human-induced pluripotent stem cell culture and generation of cortical projection neurons

Human embryonic stem cell research and protocols were approved by the Ethics Committee of the University of Liège (no. B70720096466); all experiments were conducted according to its guidelines. Human-induced pluripotent stem cell (hIPSC) line GM23446 (Coriell Institute) was maintained on Geltrex-coated dishes (Gibco) in DMEM/F12 supplemented with 20% KO serum replacement (Gibco), 100 μM nonessential amino acids (NEAA) (Gibco), 100 μM 2-mercaptoethanol, and basic fibroblast growth factor (100 ng/ml; PeproTech, London, UK), conditioned on γ-irradiated mouse embryonic fibroblasts. Cells were passaged routinely with collagenase A (1 mg/ml; Roche).

Generation of human cortical neurons was performed as described in (*39*). Briefly, hiPSCs were dissociated with TrypLE (Gibco) for 4 min at 37°C and cultured on Geltrex-coated dished in Pluripro medium (Cell Guidance Systems) until they reached confluency. Neural induction was triggered with media making use of dual SMAD inhibition and tankyrase inhibitor to enhance forebrain fate: DMEM/F12 containing N2 (Gibco), B27 (Gibco), penicillin/streptomycin (1:100; Gibco), glucose (0.8 mg/ml; Carl Roth HN06.2), NEAA, GlutaMAX (Gibco), cyclic adenosine 3′,5′-monophosphate (0.15 ng/ml; Sigma-Aldrich, A9501-1G), 500 nM A83-01 (Miltenyi Biotec, 130-106-274), 200 nM LDN-193189 (Miltenyi Biotec, 130-103-925), and 2 μM XAV939 (Enzo Life Sciences, BML-WN100-0005). Medium was changed daily, and cells were passaged at day 8 with 0.5 M EDTA. Cells were maintained until day 18 and replated at a density of 12,000 cells/cm$^2$ in neural differentiation media containing 1:1 DMEM/F12/Neurobasal, N2, B27, penicillin/streptomycin, glucose (0.8 mg/ml), NEAA, and GlutaMAX. Neural differentiation media were changed every other day, and Geltrex (1:100) was added 4 days before fixation with 4% paraformaldehyde (PFA) at day 32 to prevent detachment of the neurons.

### Immunofluorescence

Mouse cerebral cortical neurons, N2A cells, HeLa S3 cells, and human projection neurons derived from hiPSCs were fixed using 4% PFA for 20 min at room temperature (RT) and washed with phosphate-buffered saline (PBS) + 0.3% Triton X-100. Antigen retrieval was performed for nucleofected cerebral cortical neurons using 10 mM sodium citrate (pH 9) for 1 hour at 60°C. After washing, neurons were incubated in blocking solution (PBS + 0.3% Triton X-100 + 10% normal donkey serum) for 1 hour at RT. Following overnight incubation with primary antibodies (Table 1) in blocking solution at 4°C, washing, incubation with secondary antibodies (PBS + 0.3% Triton X-100 + 1% normal donkey serum) at RT for 1 hour, and washing, coverslips were mounted on a microscope slide using Mowiol.

*D. melanogaster* larvae were dissected in PBS to expose brain and motor neurons, after dissection larvae were fixed with 4% PFA for 20 min at RT, washed with PBS + 0.2% (CSP staining) or 0.3% (α-tubulin acetylation staining) Triton X-100, and incubated in blocking solution PBS and 0.2% (CSP staining) or 0.3% (α-tubulin acetylation staining) Triton X-100 + 1% bovine serum albumin (BSA) for 30 min at RT. Following overnight incubation with primary antibodies at 4°C, washing, and incubation with secondary antibodies at RT for 2 hours, the larvae were mounted on a microscope slide using Mowiol. After washing in PBS + 0.3% Triton X-100, samples were incubated in blocking solution (PBS + 5% normal donkey serum + 0.3% Triton X-100) for 1 hour at RT. Following overnight incubation with antibodies at 4°C, washing, and incubation with secondary antibodies at RT for 2 hours, the larvae were mounted on a microscope slide using Mowiol. Images were acquired with a Nikon A1Ti confocal microscope (60× lens) for all analyses, except ATAT1-GFP and BDNF-mCherry staining that was acquired with the Airyscan superresolution module of a Zeiss LSM 880 confocal microscope. HeLa cells were plated at densities of 10,000 for 96-well black-bottom plates. The following day, cells were transfected using calcium phosphate with 0.01 μg/96-well plates of ATAT1:IRES-GFP truncated-form plasmids. Twenty-four hours after transfection, cells were fixed using 4% PFA and blocked and permeabilized using PBS + 3% fetal bovine saline (FBS) + 0.1% Triton X-100 for 1 hour. Following overnight incubation with primary [total α/β-tubulin (ATN02-A) and acetylated α-tubulin (T9026)] antibodies at 4°C, washing, and incubation with secondary antibodies at RT for 2 hours, cells were imaged using an IN Cell 2200 microscope (GE Healthcare).

### Western blotting

Mouse brain cortices from *Atat1* KO mice (*20*) or HEK293 or N2A cells were homogenized on ice in radioimmunoprecipitation assay buffer or 320 mM sucrose, 4 mM Hepes buffer for subcellular fractions, with protease inhibitor cocktail (Roche, P8340 or Sigma-Aldrich, S8820) and 5 μM trichostatin A (Sigma-Aldrich, T8552). Subsequently, samples were boiled and reduced by 5 min of incubation at 70°C with loading buffer and were loaded on SDS–polyacrylamide gel electrophoresis gel to be finally transferred to a nitrocellulose membrane. For α-tubulin acetylation analysis, 2 μg of protein lysate was loaded on a gel; for analysis of all other proteins, 30 μg of lysate was used. Membranes were imaged using Amersham Imager 600 (General Electric, 29083461), and band densitometry was measured using ImageJ.

### Subcellular fractionation

Subcellular fractionation of a frozen mouse brain cortex or cultured HEK293 cells was performed as previously described (*24*).

### MS analysis

All chemicals were purchased from Sigma-Aldrich unless stated otherwise. Pellets from three independent samples of vesicles isolated from the brain cortex of WT or *Atat1* KO mice were solubilized using 5% SDS. Samples were then loaded onto the commercial S-Trap columns (ProtiFi, USA); for washing the detergents, reduction with 5 mM dithiothreitol (DTT), 10 mM iodoacetamide, and overnight digestion with trypsin (Promega) at 50:1 protein:trypsin ratio. Eluted peptides were dried using a vacuum centrifuge and stored in −80°C. Ultra LC/MS grade solvents were used for all chromatographic steps. Each sample was loaded using splitless nano ultraperformance LC (UPLC) (10 kpsi nanoACQUITY; Waters Corporation, Milford, MA, USA). The mobile phase was as follows: (A) $H_2O$ + 0.1% formic acid and (B) acetonitrile + 0.1% formic acid. Desalting of the samples was performed online using a Reversed-Phase Symmetry C18 trapping column (internal diameter of 180 μm, 20 mm in length,

and 5 μm particle size; Waters Corporation). The peptides were then separated using a T3 High Strength Silica nanocolumn (internal diameter of 75 μm, 250 mm in length, and 1.8-μm particle size; Waters Corporation) at 0.35 μl/min. Peptides were eluted from the column into the mass spectrometer using the following gradient: 4 to 30% B in 155 minutes, 30 to 90% B in 5 min, maintained at 90% for 5 min, and then back to initial conditions. The nanoUPLC was coupled online through a nanoelectrospray ionization emitter (10-μm tip; New Objective, Woburn, MA, USA) to a quadrupole orbitrap mass spectrometer (Q Exactive Plus, Thermo Fisher Scientific), using a FlexIon nanospray apparatus (Proxeon). Data were acquired in a data-dependent acquisition mode, using a top 10 method. MS1 resolution was set to 70,000 [at 200 mass/charge ratio (*m*/*z*)], mass range of 300 to 1650 *m*/*z*, and AGC of 3e6, and maximum injection time was set to 60 ms. MS2 resolution was set to 17,500, quadrupole isolation 1.7 *m*/*z*, AGC of 1e5, dynamic exclusion of 60 s, and maximum injection time of 60 ms. Raw data were processed with MaxQuant v1.6.0.16. The data were searched with the Andromeda search engine against the SwisssProt human proteome database appended with common lab protein contaminants and the following modifications: carbamidomethyl on C and oxidation of M. Quantification was based on the Label-free quantitation method, based on unique peptides. *t* test with the Holm-Sidak method for multiple comparison was used for determination of statistical significance after logarithmic transformation. GO data analysis of the differentially detected proteins was done using GOrilla tool (*40*) (http://cbl-gorilla.cs.technion.ac.il), using two ranked lists and a *P* value of $10 \times 10^{-3}$ as threshold.

### Proteinase K sensitivity assay

Proteinase K sensitivity assay was performed as previously described (*26*). Fifty micrograms of vesicles (P3) were incubated with increasing concentration of proteinase K to reach a final concentration of 0, 0.05, 0.25, 1.25, and 6.25 μg/μl in digestion buffer (10 mM Hepes, 10 mM KCL, 2 mM EGTA, and 300 mM sucrose) in a total volume of 50 μl, for 30 min at 37°C. To end the reactions, 5 mM phenylmethylsulfonyl fluoride (PMSF) with Laemmli buffer, followed by immediate boiling and reduction of the samples in 95°C for 5 min.

### Microfluidics device fabrication and axonal transport recordings in mice cortical neurons and *Drosophila* third-instar larvae

Microfluidics devices were prepared as described in (*41*). Axonal transport recording was performed after 5 DIV, as previously described (*16*), using an inverted confocal microscope (Nikon, A1Ti), at a 600-ms interval for 60 s using 60× lens. For cell culture, the recording microscope chamber was heated at 37°C and supplied with 5% $CO_2$.

### Locomotor activity and climbing assay

Larval locomotion assays were performed by placing third-instar *D. melanogaster* larvae in the center of 15-cm petri dishes coated with 3% agar (*42*). Millimeter paper was glued below each 15-cm petri dish to quantify distance traveled. Crawling speed was extrapolated from distance traveled in 1 min; peristaltic activity was defined as complete posteroanterior contraction of the larvae in 1 min. Climbing assay for adult flies was performed as previously described in (*43*). Ten flies per group were allowed to climb an empty polystyrene tube for 1 min in three sequential assays. Climbing index was defined as average ratio successful climbs over 15 cm of the total number of flies in a group.

### Lysosome transport analysis in organotypic slice

Mice purchased from Janvier were anesthetized with isoflurane (Abbott Laboratories) in an oxygen carrier before the administration of temgesic (Schering-Plough). Endotoxin-free plasmids were injected into lateral ventricles of E14.5 mouse embryo forebrains using a FemtoJet microinjector (Eppendorf) with 0.1% fast green for visualization. Injection was followed by electroporation (5 pulses of 24 mV at 50-ms intervals for 950 ms) using platinum electrodes (Sonidel, catalog no. CUY650P3) connected to an electroporator (ECM 830, BTX). Embryos were coelectroporated with tamoxifen-inducible CreERT2 expressing plasmid along with two Cre-dependent constructs expressing DsRed and shAtat1/sh-scrambled and with LAMP1-Emerald–expressing plasmid. After electroporation, embryos were placed back in the abdominal cavity. For injection, 4OHT and progesterone were dissolved in ethanol 100% at concentrations of 20 and 10 mg/ml, respectively, and then diluted with nine volumes of corn oil (Sigma-Aldrich). Diluted tamoxifen solution (2 mg/ml, 100 μl per mouse) was intraperitoneally injected three times at E17, E18, and P1, and pups brains were dissected at P2. Brains were embedded in agarose 4% HBSS solution and cut into coronal sections (300 μm) using a vibratome (Leica VT1000S, Leica Microsystems). The slices were placed on Matrigel-coated (Corning) MatTek glass-bottom dishes and covered with half-diluted Matrigel with supplemented Neurobasal culture medium. Sections were incubated for 30 min at 37°C before imaging. Time-lapse imaging was performed on a Zeiss Super Resolution LSM 880 Airyscan Elyra S1 (×63 magnification) at a 500-ms interval for 60 s at the corpus callosum midline. The recoding microscope chamber was heated at 37°C and supplied with 5% $CO_2$.

### qPCR analysis

Ten adult fly heads were collected in TRIzol Reagent (Ambion, Life Technologies), followed by RNA extraction performed using the manufacturer's instructions. After deoxyribonuclease treatment (Roche), 1 μg of RNA was reverse-transcribed with RevertAid Reverse Transcriptase (Fermentas). qPCR was performed using a LightCycler 480 (Roche), with SYBR Green mix according to the manufacturer's instructions (Roche). Analysis was done using $2^{-\Delta\Delta}$CT method after defining primer efficiencies, *Rpl13* and *Pgk* served for normalization (*44*). The following primers were used: *Rpl13*, AGGAGGCGCAAGAAATC (forward) and CTTGCTGCGGTACTCCTTGAG (reverse); *Pgk*, TCCTGAAGGTCCTCAACAACATG (forward) and TCCACCAGTTTCTCGACGATCT (reverse); *Atat1*, CAGTCCCGCACGCTGACGAG (forward) and ACGCGCATGGTGGAGCAGAC (reverse); *Atat2*, TCCCAAGTCAAGGGAGACAC (forward) and TGCGGAAAGAGGTGCTTAAT (reverse); and *Hdac6*, CAAGCCCAAAGTCAAGCACT (forward) and ACCCAGTTCTCCCCCGTC (reverse).

#### *Ciliobrevin treatment*

Drug treatments of cortical neuronal cultures were performed using 20 μM (Sigma-Aldrich 250401) diluted in dimethyl sulfoxide (DMSO) for 2 hours. For third-instar larva, drugs were fed in 10% sucrose solution supplemented with either 1 mM TBA (Sigma-Aldrich, SML0044) or 800 μM Ciliobrevin D and DMSO for 30 min and 2 hours, respectively.

### Purification of tubulin from mouse brains or HeLa cells

Nonacetylated α-tubulin was obtained from HeLa S3 cells (American Type Culture Collection, CCL-2.2TM) for in vitro acetylation assays

or from WT and *Atat1* KO mouse brains for in vitro transport assay according to the protocol adapted from (*45*). Cells were lysed in BRB80 [80 mM $K^-$ Pipes (pH 6.8), 1 mM $MgCl_2$, and 1 mM EGTA] supplemented with 1 mM β-mercaptoethanol, 1 mM PMSF, and protease inhibitors at 4°C. The soluble fraction was obtained by ultracentrifugation, followed by tubulin polymerization at 30°C min by adding 1 mM guanosine triphosphate (GTP) and 30% glycerol. MTs were pelleted by ultracentrifugation at 30°C for 30 min and depolymerized in BRB80 at 4°C; soluble tubulin was clarified by ultracentrifugation at 4°C. The second polymerization round was performed for 30 min at 30°C in the presence of high-molarity Pipes to remove mitogen-activated proteins; the MT pellet was sedimented by ultracentrifugation. MTs were then depolymerized in BRB80 at 4°C, and soluble tubulin was clarified and snap-frozen.

### In vitro α-tubulin acetylation assays

Half-area 96-well plates (Greiner, 674061) were coated with 5-μg tubulin from HeLa cells or bovine brain (Cytoskeleton, catalog no. HTS02-A) in 25 μl of ultrapure water for 2.5 hours at 37°C, followed by blocking (PBS + 3% BSA + 3% skim milk + 3% FBS) for 1 hour at 37°C, and washing with PBS + 0.05% Tween 20. Twenty-five micrograms of the total, S2, S3, or P3 fractions isolated from the P0 mouse brain cortex were diluted in 2× histone acetyltransferase (HAT) buffer (Sigma-Aldrich, EPI001A) supplemented with protease inhibitor cocktail, 5 μM trichostatin, and 50 μM acetyl-CoA (Sigma-Aldrich, A2056) or vehicle ($H_20$) were added per well for incubation of 2 hours at 37°C with shaking at 100 revolutions per minute. The wells were washed and incubated overnight with acetylated α-tubulin antibody (1:2000) in blocking buffer (PBS + 0.05% Tween 20 + 3% BSA) at 4°C, and wells were washed and incubated for 2 hours at 37°C with peroxidase-conjugated goat anti-mouse antibody (1:5000) in antibody blocking buffer; following another wash, the samples were incubated with trimethylboron/E (Merck Millipore, ES001), and the reaction was stopped with $H_2SO_4$.

CoA release was measured using HAT activity colorimetric assay kit (Sigma-Aldrich, EPI001), as indicated by the manufacturer's instructions. Twenty-five micrograms of P3 fraction were incubated with 5 μg of tubulin in black-bottom μClear plate (Greiner, 655090) for 4 hours, and signal was measured every minute.

### In vitro MT-dependent transport assay

WT or *Atat1* KO mouse brain was fractionated in vesicle buffer [10 mM Hepes-KOH, 175 mM L-aspartic acid, 65 mM taurine, 85 mM betaine, 25 mM glycine, 6.5 mM $MgCl_2$, 5 mM EGTA, 0.5 mM D-glucose, 1.5 mM $CaCl_2$, and 20 mM DTT (pH 7.2), with protease inhibitors], using increasing centrifugation speed with a final sucrose gradient step to isolate motility vesicles as described in (*23*). Rhodamine-labeled seeds were prepared by incubating a mix of rhodamine labeled with unlabeled purified tubulin from bovine brain (Cytoskeleton, catalog no. HTS02-A) or HeLa cells (isolated as described above) at a ratio of 1:10 for 1 hour at 37°C. The elongation was carried in GTP-BRB80 buffer (80 mM Pipes, 1 mM $MgCl_2$, 1 mM EGTA, and 1 mM GTP) for 30 min at 37°C, followed by incubation for 20 min with 50 μM Taxol to stabilize MTs.

The in vitro polymerized rhodamine-labeled MTs from WT or *Atat1* KO mouse brains were seeded in a flow chamber and purified vesicles diluted in motility buffer [BRB80, 0.5% Pluronic F127, 1 mM Taxol, BSA in BRB80 (10 mg/ml), 1 M DTT, glucose oxidase (0.5 mg/ml), 20 mM Mg-ATP, glucose (15 mg/ml), and catalase (470 U/ml)] were labeled with the green fluorescent lipophilic carbocyanine [DiOC18(3), Thermo Fisher Scientific] tracer, loaded in the chambers with 50 μM acetyl-CoA or vehicle, to acquire using a total internal reflection fluorescence (TIRF) microscope. For immunofluorescence analysis, MTs were fixed after the assay with 100% methanol for 10 min at −20°C, then incubated in blocking solution (PBS + 1% BSA) with acetylated α-tubulin antibody (1:10,000) and goat anti-mouse Alexa 647 antibody (1:1000) for 2 hours at RT. Recordings were performed by using a TIRF microscope (Nikon, Eclipse Ti), at 200-ms intervals, using 60× lens.

### Quantification of MT acetylation levels using immunofluorescence

Fluorescence intensity levels were measured by Fiji (https://imagej.net/Fiji/Downloads). Regions of interest of 30 μm long for *D. melanogaster*, or the complete length for in vitro polymerized MTs, accounting for the full width of the motoneurons/MTs were used. The levels of acetylated α-tubulin and total α-tubulin levels were extracted from mean intensity levels. Background levels were subtracted, and the ratio of acetylated α-tubulin/tubulin was calculated.

### Analysis of MT-dependent transport

Kymographs were generated for single blind analysis using ImageJ plugin-KymoToolBox (fabrice.cordelieres@curie.u-psud.fr). For *D. melanogaster* analysis, StackReg plugin was used to align frames. Vesicles were considered stationary if speed was lower than 0.1 μm/s.

### Statistics

All experiments (except WB and quantitative reverse transcription PCR analyses) were performed under single-blinded condition, and statistical analyses were generated with GraphPad Prism Software 6.0 or GraphPad Prism Software 7.0 for proteomic analysis.

## SUPPLEMENTARY MATERIALS

Supplementary material for this article is available at http://advances.sciencemag.org/cgi/content/full/5/12/eaax2705/DC1

Fig. S1. Analysis of axonal transport parameters in WT and Atat1 KO mice.
Fig. S2. Validation of RNAi efficiency, mRNA expression of MTs modifying enzymes, representative kymographs of axonal transport, and protein aggregation in *D. melanogaster*.
Fig. S3. Kymographs of in vitro transport assay.
Fig. S4. Identified peptides of ATAT1 by LC-MS/MS.
Fig. S5. LC-MS/MS proteomics on vesicular extracts from WT and ATAT1 KO mice.
Fig. S6. Acute KD of Lis1 leads to defect in retrograde transport and dampens the acetylation of MTs.
Fig. S7. Expression of Atat1 in the cerebral cortex of human in the course of development and life.
Table S1. Intensity-ranked proteins in vesicle fractions from WT or Atat1 KO mice detected by LC-MS/MS.
Table S2. Differentially detected proteins in vesicle fractions from WT or Atat1 KO mice detected by LC-MS/MS.
Table S3. Identified molecular motors in vesicle fractions from WT or Atat1 KO mice detected by LC-MS/MS.
Table S4. Identified glycolytic enzymes in vesicle fractions from WT or Atat1 KO mice detected by LC-MS/MS.
Movie S1. Representative movie of Lamp1-Emerald trafficking in axons of cortical brain slice.
Movie S2. Representative movie of lysosome trafficking in axons located in the distal part of PDMS chambers.
Movie S3. Representative movie of mitochondria trafficking in axons located in the distal part of PDMS chambers.
Movie S4. Representative movie of synaptotagmin-GFP trafficking in motoneurons of third-instar larvae.
Movie S5. Representative movies of vesicles trafficking in vitro over polymerized rhodamine-labeled MTs.
Movie S6. Representative movie of ATAT1-GFP trafficking in axons located in the distal part of PDMS chambers.

View/request a protocol for this paper from *Bio-protocol*.

## REFERENCES AND NOTES


1. N. Hirokawa, S. Niwa, Y. Tanaka, Molecular motors in neurons: Transport mechanisms and roles in brain function, development, and disease. *Neuron* **68**, 610–638 (2010).
2. C. Janke, J. C. Bulinski, Post-translational regulation of the microtubule cytoskeleton: Mechanisms and functions. *Nat. Rev. Mol. Cell Biol.* **12**, 773–786 (2011).
3. Y. Song, S. T. Brady, Post-translational modifications of tubulin: Pathways to functional diversity of microtubules. *Trends Cell Biol.* **25**, 125–136 (2015).
4. J. P. Dompierre, J. D. Godin, B. C. Charrin, F. P. Cordelières, S. J. King, S. Humbert, F. Saudou, Histone deacetylase 6 inhibition compensates for the transport deficit in Huntington's disease by increasing tubulin acetylation. *J. Neurosci.* **27**, 3571–3583 (2007).
5. N. A. Reed, D. Cai, T. L. Blasius, G. T. Jih, E. Meyhofer, J. Gaertig, K. J. Verhey, Microtubule acetylation promotes kinesin-1 binding and transport. *Curr. Biol.* **16**, 2166–2172 (2006).
6. V. K. Godena, N. Brookes-Hocking, A. Moller, G. Shaw, M. Oswald, R. M. Sancho, C. C. J. Miller, A. J. Whitworth, K. J. De Vos, Increasing microtubule acetylation rescues axonal transport and locomotor deficits caused by LRRK2 Roc-COR domain mutations. *Nat. Commun.* **5**, 5245 (2014).
7. J. S. Akella, D. Wloga, J. Kim, N. G. Starostina, S. Lyons-Abbott, N. S. Morrissette, S. T. Dougan, E. T. Kipreos, J. Gaertig, MEC-17 is an α-Tubulin acetyltransferase. *Nature* **467**, 218–222 (2010).
8. T. Shida, J. G. Cueva, Z. Xu, M. B. Goodman, M. V. Nachury, The major α-Tubulin K40 acetyltransferase α-TAT1 promotes rapid ciliogenesis and efficient mechanosensation. *Proc. Natl. Acad. Sci. U.S.A.* **107**, 21517–21522 (2010).
9. S. C. Howes, G. M. Alushin, T. Shida, M. V. Nachury, E. Nogales, Effects of tubulin acetylation and tubulin acetyltransferase binding on microtubule structure. *Mol. Biol. Cell* **25**, 257–266 (2014).
10. Z. Xu, L. Schaedel, D. Portran, A. Aguilar, J. Gaillard, M. P. Marinkovich, M. Théry, M. V. Nachury, Microtubules acquire resistance from mechanical breakage through intralumenal acetylation. *Science* **356**, 328–332 (2017).
11. C. Coombes, A. Yamamoto, M. M. Clellan, T. A. Reid, M. Plooster, G. W. G. Luxton, J. Alper, J. Howard, M. K. Gardner, Mechanism of microtubule lumen entry for the α-Tubulin acetyltransferase enzyme αTAT1. *Proc. Natl. Acad. Sci. U.S.A.* **113**, E7176–E7184 (2016).
12. N. Ly, N. Elkhatib, E. Bresteau, O. Piétrement, M. Khaled, M. M. Magiera, C. Janke, E. L. Cam, A. D. Rutenberg, G. Montagnac, αTAT1 controls longitudinal spreading of acetylation marks from open microtubules extremities. *Sci. Rep.* **6**, 35624 (2016).
13. L. Balabanian, C. L. Berger, A. G. Hendricks, Acetylated microtubules are preferentially bundled leading to enhanced kinesin-1 motility. *Biophys. J.* **113**, 1551–1560 (2017).
14. G. W. Kim, L. Li, M. Gorbani, L. You, X. J. Yang, Mice lacking α-Tubulin acetyltransferase 1 are viable but display α-Tubulin acetylation deficiency and dentate gyrus distortion. *J. Biol. Chem.* **288**, 20334–20350 (2013).
15. T. Shida, J. G. Cueva, Z. Xu, M. B. Goodman, M. V. Nachury, The major α-Tubulin K40 acetyltransferase αTAT1 promotes rapid ciliogenesis and efficient mechanosensation. *Proc. Natl. Acad. Sci. U.S.A.* **107**, 21517–21522 (2010).
16. G. Morelli, A. Even, I. Gladwyn-Ng, R. L. Bail, M. Shilian, J. D. Godin, E. Peyre, B. A. Hassan, A. Besson, J.-M. Rigo, M. Weil, B. Brône, L. Nguyen, $p27^{Kip1}$ Modulates Axonal Transport by Regulating α-Tubulin Acetyltransferase 1 Stability. *Cell Rep.* **23**, 2429–2442 (2018).
17. C. Hubbert, A. Guardiola, R. Shao, Y. Kawaguchi, A. Ito, A. Nixon, M. Yoshida, X.-F. Wang, T.-P. Yao, HDAC6 is a microtubule-associated deacetylase. *Nature* **417**, 455–458 (2002).
18. K. V. Butler, J. Kalin, C. Brochier, G. Vistoli, B. Langley, A. P. Kozikowski, Rational design and simple chemistry yield a superior, neuroprotective HDAC6 inhibitor, tubastatin A. *J. Am. Chem. Soc.* **132**, 10842–10846 (2010).
19. C. D. Nichols, J. Becnel, U. B. Pandey, Methods to assay Drosophila behavior. *J. Vis. Exp.* **7**, 3795 (2012).
20. N. Kalebic, S. Sorrentino, E. Perlas, G. Bolasco, C. Martinez, P. A. Heppenstall, αTAT1 is the major α-Tubulin acetyltransferase in mice. *Nat. Commun.* **4**, 1962 (2013).
21. S. Takamori, M. Holt, K. Stenius, E. A. Lemke, M. Grønborg, D. Riedel, H. Urlaub, S. Schenck, B. Brügger, P. Ringler, S. A. Müller, B. Rammner, F. Gräter, J. S. Hub, B. L. De Groot, G. Mieskes, Y. Moriyama, J. Klingauf, H. Grubmüller, J. Heuser, F. Wieland, R. Jahn, Molecular Anatomy of a Trafficking Organelle. *Cell* **127**, 831–846 (2006).
22. G. H. H. Borner, M. Harbour, S. Hester, K. S. Lilley, M. S. Robinson, Comparative proteomics of clathrin-coated vesicles. *J. Cell Biol.* **175**, 571–578 (2006).
23. M.-V. Hinckelmann, A. Virlogeux, C. Niehage, C. Poujol, D. Choquet, B. Hoflack, D. Zala, F. Saudou, Self-propelling vesicles define glycolysis as the minimal energy machinery for neuronal transport. *Nat. Commun.* **7**, 13233 (2016).
24. D. Zala, M.-V. Hinckelmann, H. Yu, M. M. L. da Cunha, G. Liot, F. P. Cordelières, S. Marco, F. Saudou, Vesicular glycolysis provides on-board energy for fast axonal transport. *Cell* **152**, 479–491 (2013).
25. G. Montagnac, V. Meas-Yedid, M. Irondelle, A. Castro-Castro, M. Franco, T. Shida, M. V. Nachury, A. Benmerah, J.-C. Olivo-Marin, P. Chavrier, αTAT1 catalyses microtubule acetylation at clathrin-coated pits. *Nature* **502**, 567–570 (2013).
26. H.-J. Lee, S. Patel, S.-J. Lee, Intravesicular localization and exocytosis of α-synuclein and its aggregates. *J. Neurosci.* **25**, 6016–6024 (2005).
27. R. Sainath, G. Gallo, The dynein inhibitor Ciliobrevin D inhibits the bidirectional transport of organelles along sensory axons and impairs NGF-mediated regulation of growth cones and axon branches. *Dev. Neurobiol.* **75**, 757–777 (2015).
28. B. Neumann, M. A. Hilliard, Loss of MEC-17 leads to microtubule instability and axonal degeneration. *Cell Rep.* **6**, 93–103 (2014).
29. S. J. Morley, Y. Qi, L. Iovino, L. Andolfi, D. Guo, N. Kalebic, L. Castaldi, C. Tischer, C. Portulano, G. Bolasco, K. Shirlekar, C. M. Fusco, A. Asaro, F. Fermani, M. Sundukova, U. Matti, L. Reymond, A. De Ninno, L. Businaro, K. Johnsson, M. Lazzarino, J. Ries, Y. Schwab, J. Hu, P. A. Heppenstall, Acetylated tubulin is essential for touch sensation in mice. *eLife* **5**, e20813 (2016).
30. L. Li, D. Wei, Q. Wang, J. Pan, R. Liu, X. Zhang, L. Bao, MEC-17 deficiency leads to reduced α-Tubulin acetylation and impaired migration of cortical neurons. *J. Neurosci.* **32**, 12673–12683 (2012).
31. J. A. Miller, S.-L. Ding, S. M. Sunkin, K. A. Smith, L. Ng, A. Szafer, A. Ebbert, Z. L. Riley, J. J. Royall, K. Aiona, J. M. Arnold, C. Bennet, D. Bertagnolli, K. Brouner, S. Butler, S. Caldejon, A. Carey, C. Cuhaciyan, R. A. Dalley, N. Dee, T. A. Dolbeare, B. A. C. Facer, D. Feng, T. P. Fliss, G. Gee, J. Goldy, L. Gourley, B. W. Gregor, G. Gu, R. E. Howard, J. M. Jochim, C. L. Kuan, C. Lau, C.-K. Lee, F. Lee, T. A. Lemon, P. Lesnar, B. M. Murray, N. Mastan, N. Mosqueda, T. Naluai-Cecchini, N.-K. Ngo, J. Nyhus, A. Oldre, E. Olson, J. Parente, P. D. Parker, S. E. Parry, A. Stevens, M. Pletikos, M. Reding, K. Roll, D. Sandman, M. Sarreal, S. Shapouri, N. V. Shapovalova, E. H. Shen, N. Sjoquist, C. R. Slaughterbeck, M. Smith, A. J. Sodt, D. Williams, L. Zöllei, B. Fischl, M. B. Gerstein, D. H. Geschwind, I. A. Glass, M. J. Hawrylycz, R. F. Hevner, H. Huang, A. R. Jones, J. A. Knowles, P. Levitt, J. W. Phillips, N. Šestan, P. Wohnoutka, C. Dang, A. Bernard, J. G. Hohmann, E. S. Lein, Transcriptional landscape of the prenatal human brain. *Nature* **508**, 199–206 (2014).
32. I. A. Kent, P. S. Rane, R. B. Dickinson, A. J. Ladd, T. P. Lele, Transient pinning and pulling: A mechanism for bending microtubules. *PLOS ONE* **11**, e0151322 (2016).
33. A. D. Bicek, E. Tüzel, A. Demtchouk, M. Uppalapati, W. O. Hancock, D. M. Kroll, D. J. Odde, Anterograde microtubule transport drives microtubule bending in LLC-PK1 epithelial cells. *Mol. Biol. Cell* **20**, 2943–2953 (2009).
34. S. Triclin, D. Inoue, J. Gaillard, Z. M. Htet, M. De Santis, D. Portran, E. Derivery, C. Aumeier, L. Schaedel, K. John, C. Leterrier, S. Reck-Peterson, L. Blanchoin, M. Thery, Self-repair protects microtubules from their destruction by molecular motors. *bioRxiv* , 499020 (2018).
35. J. F. Díaz, I. Barasoain, J. M. Andreu, Fast kinetics of Taxol binding to microtubules. Effects of solution variables and microtubule-associated proteins. *J. Biol. Chem.* **278**, 8407–8419 (2003).
36. D. Portran, L. Schaedel, Z. Xu, M. Théry, M. V. Nachury, Tubulin acetylation protects long-lived microtubules against mechanical ageing. *Nat. Cell Biol.* **19**, 391–398 (2017).
37. M.-V. Hinckelmann, D. Zala, F. Saudou, Releasing the brake: Restoring fast axonal transport in neurodegenerative disorders. *Trends Cell Biol.* **23**, 634–643 (2013).
38. J. W. Tsai, Y. Chen, A. R. Kriegstein, R. B. Vallee, LIS1 RNA interference blocks neural stem cell division, morphogenesis, and motility at multiple stages. *J. Cell Biol.* **170**, 935–945 (2005).
39. V. Iefremova, G. Manikakis, O. Krefft, A. Jabali, K. Weynans, R. Wilkens, F. Marsoner, B. Brändl, F.-J. Müller, P. Koch, J. Ladewig, An organoid-based model of cortical development identifies non-cell-autonomous defects in Wnt signaling contributing to miller-dieker syndrome. *Cell Rep.* **19**, 50–59 (2017).
40. E. Eden, R. Navon, I. Steinfeld, D. Lipson, Z. Yakhini, *GOrilla*: A tool for discovery and visualization of enriched GO terms in ranked gene lists. *BMC Bioinformatics* **10**, 48 (2009).
41. S. Gluska, M. Chein, N. Rotem, A. Ionescu, E. Perlson, Tracking Quantum-Dot labeled neurotropic factors transport along primary neuronal axons in compartmental microfluidic chambers. *Methods Cell Biol.* **131**, 365–387 (2016).
42. S. A. Shaver, C. A. Riedl, T. L. Parkes, M. B. Sokolowski, A. J. Hilliker, Isolation of larval behavioral mutants in Drosophila melanogaster. *J. Neurogenet.* **14**, 193–205 (2000).
43. R. P. Chambers, G. B. Call, D. Meyer, J. Smith, J. A. Techau, K. Pearman, L. M. Buhlman, Nicotine increases lifespan and rescues olfactory and motor deficits in a Drosophila model of Parkinson's disease. *Behav. Brain Res.* **253**, 95–102 (2013).
44. G. Morelli, A. Avila, S. Ravanidis, N. Aourz, R. L. Neve, I. Smolders, R. J. Harvey, J.-M. Rigo, L. Nguyen, B. Brône, Cerebral cortical circuitry formation requires functional glycine receptors. *Cereb. Cortex* **27**, 1863–1877 (2016).
45. M. Barisic, R. S. e Sousa, S. K. Tripathy, M. M. Magiera, A. V. Zaytsev, A. L. Pereira, C. Janke, E. L. Grishchuk, H. Maiato, Mitosis. Microtubule detyrosination guides chromosomes during mitosis. *Science* **348**, 799–803 (2015).


**Acknowledgments:** We thank B. Franco (ULiège) and S. Bodakuntla (Institut Curie) for technical assistance; M. Nachury for sharing ATAT1 antibody and K. Sadoul for providing the *Atat1* KO mice; Y. Levin from The de Botton Protein Profiling Institute of the Nancy and Stephen Grand Israel National Center for Personalized Medicine, Weizmann Institute of Science for the proteomic analysis; F. Polleux, from Columbia University, New York, USA, for providing pCAG mEmerald-LAMP1, and pCAG mito-DsRED plasmids; and E. Even for graphical

design. **Funding:** A.E.'s stay at GIGA Research Institute of the University of Liège was funded by EMBO Short-Term Fellowships (ASTF 174-2016); his stay at F.S.'s lab was supported by TAU Global Research and Training Fellowship, Ela Kodesz Institute, and the Scientific and Academic Cooperation Office of the French embassy in Tel Aviv. A.E., M.S., and M.W.'s research was supported by the Israel Science Foundation (grant no. 1688/16). C.S. was supported by a Postdoctoral fellowship from FRM and by EMBO LTF (ALTF 693-2015). S.T., L.B., L.N., and B.M. are PhD fellow, Postdoctoral fellow, Senior Research Associates and Director from FRS-FNRS, respectively. This work was supported by the FRS-FNRS, the Fonds Léon Fredericq (L.N. and B.M.), the Fondation Médicale Reine Elisabeth (L.N. and B.M.), the Fondation Simone et Pierre Clerdent (L.N.), the Belgian Science Policy [IAP-VII network P7/20 (L.N.) and IAP-VII network P7/10 (B.B.)], and the ERANET Neuron STEM-MCD and NeuroTalk (L.N.); grants from Agence Nationale de la Recherche [ANR-14-CE35-0027-01 PASSAGE (F.S.), ANR-15-JPWG-0003-05 JPND CIRCPROT (F.S.), ANR-15-IDEX-02 NeuroCoG (F.S.), ANR-10-IDEX-0001-02, and ANR-11-LBX-003 (C.J.) in the framework of the "Investissements d'avenir" program]; the LABEX celtisphybio 8 (C.J.); and the Fondation pour la Recherche Médicale (FRM, équipe labellisée, to F.S.). C.J. is supported by the Institut Curie, the French National Research Agency (ANR) award ANR-17-CE13-0021 and the Fondation pour la Recherche Medicale (FRM) grant DEQ20170336756. J.A.S. was supported by the European Union's Horizon 2020 research and innovation program under the Marie Sklodowska-Curie grant agreement no. 675737 and the FRM grant FDT201904008210. M.M.M. was supported by the Fondation Vaincre Alzheimer (grant no. FR-16055p). **Author contributions:** A.E., G.M., F.S., M.W., and L.N. designed the study. A.E. and G.M. performed and interpreted most experiments. L.B. and S.T. designed and performed ex vivo experiments, contributed to in vitro transport experiments and superresolution imaging, and reviewed the manuscript with the help of coauthors. C.S. performed in vitro motility assays under the supervision of F.S. I.G.-N. contributed to cell cultures, transport experiment in mice, and cloning. R.L.B. contributed to *Drosophila* work. M.S. contributed to cell cultures and biochemical work. M.M.M. and A.S.J. produced and purified nonacetylated MTs. M.M.M. performed analysis of tubulin PTMs. S.F. maintained *Atat1 KO* animal colonies and contributed to cortical tissue dissections. N.K. provided technical assistance for molecular biology and mouse husbandry. M.W. and L.N. contributed to data interpretation; and A.E., G.M., M.W., and L.N. wrote the manuscript with input from all coauthors. **Competing interests:** The authors declare that they have no competing interests. **Data and materials availability:** An earlier version of the work can be found at bioRxiv 542464; doi: https://doi.org/10.1101/542464. All data needed to evaluate the conclusions in the paper are present in the paper and/or the Supplementary Materials. Additional data related to this paper may be requested from the authors.

Submitted 8 March 2019
Accepted 28 October 2019
Published 18 December 2019
10.1126/sciadv.aax2705

**Citation:** A. Even, G. Morelli, L. Broix, C. Scaramuzzino, S. Turchetto, I. Gladwyn-Ng, R. Le Bail, M. Shilian, S. Freeman, M. M. Magiera, A. S. Jijumon, N. Krusy, B. Malgrange, B. Brone, P. Dietrich, I. Dragatsis, C. Janke, F. Saudou, M. Weil, L. Nguyen, ATAT1-enriched vesicles promote microtubule acetylation via axonal transport. *Sci. Adv.* **5**, eaax2705 (2019).

Science Advances

# ATAT1-enriched vesicles promote microtubule acetylation via axonal transport

Aviel Even, Giovanni Morelli, Loïc Broix, Chiara Scaramuzzino, Silvia Turchetto, Ivan Gladwyn-Ng, Romain Le Bail, Michal Shilian, Stephen Freeman, Maria M. Magiera, A. S. Jijumon, Nathalie Krusy, Brigitte Malgrange, Bert Brone, Paula Dietrich, Ioannis Dragatsis, Carsten Janke, Frédéric Saudou, Miguel Weil and Laurent Nguyen

*Sci Adv* **5** (12), eaax2705.
DOI: 10.1126/sciadv.aax2705